Cell-Free Massive Non-Terrestrial Networks

Seungnyun Kim, *Member, IEEE*, Jiao Wu, *Member, IEEE*, Byonghyo Shim, *Senior Member, IEEE*, and Moe Z. Win, *Fellow, IEEE*

***Abstract*— As a means to provide ubiquitous connectivity across the ground-air-space 3D network, low Earth orbit (LEO) satellite mega-constellation systems comprising thousands of LEO satellites have attracted significant interest from both academia and industry recently. One major issue of LEO mega-constellation systems is the frequent handovers between satellites and beams, causing an increase in communication latency and deterioration of quality of service (QoS). In this paper, we propose a user-centric cooperative communication framework for next generation (xG) LEO satellite mega-constellation systems. In the proposed framework, a group of LEO satellites simultaneously serve all the user equipments (UEs) using the same time-frequency resources. By dynamically organizing the clusters of serving satellites and coordinating their joint transmission based on statistical channel state information (CSI), the handover frequency and inter-satellite interference can be reduced effectively, thereby achieving significant enhancements in the spectral efficiency and coverage probability. From the achievable rate analysis and extensive simulations on realistic xG LEO satellite communication environments, we show that the proposed scheme substantially improves the spectral efficiency and coverage over the conventional beam-centric systems.**

***Index Terms*— Cell-free systems, LEO satellite communications, satellite clustering, joint transmission, statistical CSI.**

I. Introduction

NEXT GENERATION (XG) wireless systems are expected to provide ubiquitous global connectivity, even for remote and challenging regions such as deserts, mountains, rural areas, and oceans [1], [2], [3], [4]. As a means to achieve this relentless goal, non-terrestrial networks (NTN) that include satellites in low Earth orbit (LEO), medium Earth orbit (MEO), and geosynchronous equatorial orbit (GEO), have gained much attention recently [5], [6], [7], [8], [9], and [10]. Since satellites can be deployed in orbits covering any location on Earth, NTN can provide pervasive and reliable connectivity across the ground-air-space 3D space. Among these, there has been a tremendous interest in LEO satellite communications within both industry and academia due to the reduced latency, enhanced signal quality, low cost, and flexible deployment [11], [12].

One major bottleneck of LEO satellite communications is that LEO satellites can cover only a small portion of the Earth's surface for a brief duration since they operate at relatively low altitudes (500-2,000 km) and move rapidly across the orbit [13]. For example, while the GEO satellite can cover one-third of the Earth's surface, the coverage (i.e., footprint) radius of the LEO satellite is 600 km. To broaden the coverage of LEO satellites, satellite constellation systems with hundreds or thousands of satellites are commonly used [14], [15]. By densely deploying LEO satellites, the coverage and system capacity can be improved substantially. In fact, for the provision of worldwide broadband services, many LEO satellite companies (e.g., Starlink, OneWeb, and Kuiper) are developing satellite mega-constellation systems comprising a massive number (more than 10,000) of satellites. For example, Starlink has already launched 5,500 satellites and anticipates expanding the number of satellites to 12,000 by the mid-2020s.

A. Prior Works

In the satellite mega-constellation systems, to provide communication services to the terrestrial and aerial user equipments (UEs), a beam-centric approach that exploits highly focused beams aimed at specific terrestrial regions (i.e., *spot beams*) has been widely used (see Fig. 1a) [16]. In this approach, each satellite sends multiple spot beams directed toward distinct areas and then the UE connects to the spot beam maximizing the received signal power. For instance, Starlink's LEO satellites are equipped with 4 phased array antennas, which generate 48 distinct spot beams. In accordance with this trend, various beam-centric communication frameworks have been proposed recently [17], [18], [19], [20], and [21]. In [17], a hybrid wide-spot beam coverage scheme that uses a combination of wide and spot beams has been proposed. In [18], a spot beam position optimization technique for LEO beam-hopping systems has been proposed. In [19], an approach to dynamically allocate spot beams according to the UE distribution has been proposed. In [20], a downlink performance of multi-beam systems has been analyzed. In [21], a dynamic beam pattern selection and user scheduling tech-

Received 15 January 2024; revised 30 June 2024; accepted 6 August 2024. Date of publication 9 December 2024; date of current version 18 December 2024. The fundamental research described in this paper was supported, in part, by the National Research Foundation of Korea under Grant RS-2023-00252789 and Grant RS-2023-00208985, by the National Science Foundation under Grant CNS-2148251, and by the federal agency and industry partners in the RINGS program. *(Corresponding author: Moe Z. Win.)*

Seungnyun Kim is with the Wireless Information and Network Sciences Laboratory, Massachusetts Institute of Technology, Cambridge, MA 02139 USA (e-mail: snkim94@mit.edu).

Jiao Wu is with the Computer, Electrical and Mathematical Sciences and Engineering Division, King Abdullah University of Science and Technology, Thuwal 23955, Saudi Arabia (e-mail: jiao.wu@kaust.edu.sa).

Byonghyo Shim is with the Institute of New Media and Communications, Seoul National University, Seoul 08826, Republic of Korea (e-mail: bshim@snu.ac.kr).

Moe Z. Win is with the Laboratory for Information and Decision Systems (LIDS), Massachusetts Institute of Technology, Cambridge, MA 02139 USA (e-mail: moewin@mit.edu).

Digital Object Identifier 10.1109/JSAC.2024.3460080

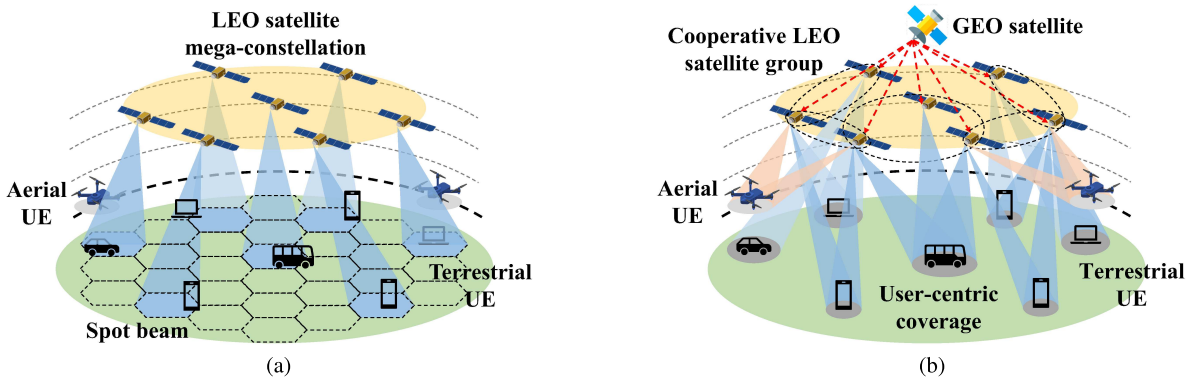

Fig. 1. Comparison between (a) the conventional beam-centric systems and (b) the proposed CF-mNTN.

nique has been proposed. Also, advanced precoding techniques have been investigated in [22], [23], [24], [25], [26], [27], and [28]. Specifically, in [22], beam pattern design and bandwidth allocation algorithms based on deep reinforcement learning (DRL) technique have been proposed. In [23], [24], and [25], hybrid analog-digital precoding techniques for massive multiple-input multiple-output (MIMO) satellite communication systems have been proposed. In [26], [27], and [28], joint precoding techniques for integrated satellite-terrestrial networks (ISTN) have been proposed. In addition to the single-satellite precoding techniques, a multi-satellite transmission framework has been proposed in [29], [30], and [31]. In [29], a distributed MIMO technique for LEO satellite networks has been proposed. In [30], a cooperative hybrid beamforming and user scheduling algorithm has been proposed. Also, in [31], a coverage analysis of the cooperative transmission scheme has been conducted.

A major issue of the conventional beam-centric approach is the frequent handovers between the spot beams (i.e., inter-beam handover) and between satellites (i.e., inter-satellite handover) [32], [33]. This arises from the facts that a UE is connected to only one spot beam at a time and the beam coverage area changes rapidly due to the high orbital speed of satellites. For example, in the Iridium systems, the coverage radius of a spot beam is 400 km and the orbital speed of LEO satellites is around 7.6 km/s, meaning that the inter-beam handover occurs every 52 seconds. Such frequent handovers will not only increase communication latency but also degrade throughput. This issue is even more serious in satellite mega-constellation systems, which comprise thousands of LEO satellites [15]. Another critical issue with the conventional beam-centric approach is the significant performance degradation of the UEs located at the footprint boundaries [34]. These cell-edge UEs suffer from reduced signal strength as well as the interferences from adjacent beams and satellites. The number of cell-edge UEs is expected to grow even larger in satellite mega-constellation systems due to the large numbers of spot beams and satellites. One exception is the multi-satellite transmission scheme in [29], [30], and [31]. While these schemes can reduce the satellite handover frequency, they rely heavily on the instantaneous channel state information (CSI), which is difficult to acquire in practice due to the large propagation delays and high mobility of LEO satellites.

The fundamental questions related to the LEO satellite mega-constellation systems are: 1) how to ensure seamless connectivity while reducing handover frequency; and 2) how to provide uniformly good quality of service (QoS) to all UEs? The answers to these questions will not only decrease handover occurrences and enhance QoS but also realize hyper-connected ground-air-space network. This, in turn, will bring to fruition immersive xG Internet-of-Things (IoT) applications such as urban air mobility (UAM), factory of the future (FoF), robotics, and maritime transportation system (MTS).

B. Our Contributions

The aim of this paper is to propose a user-centric cooperative communication framework for LEO satellite mega-constellation systems. When compared to conventional beam-centric systems where a single satellite serves only the UEs within its footprint using the regional spot beams, in the proposed *cell-free massive non-terrestrial networks* (CF-mNTN), a group of LEO satellites simultaneously serve all the UEs through joint transmission (see Fig. 1b). Since the associations between LEO satellites and UEs are not strictly limited by the regional footprint, a notion of footprint boundary is unnecessary in CF-mNTN. Also, by dynamically adjusting the satellite-UE associations and the power weights between LEO satellites and UEs according to the wireless environments, CF-mNTN can effectively control inter-satellite interferences, thereby enhancing spectral efficiency and coverage.

An intriguing feature of CF-mNTN is that it utilizes only the statistical CSI, such as angles and path loss, for the downlink precoding/decoding and power allocation. Since the statistical CSI changes at a much slower rate compared to the instantaneous CSI, the use of statistical CSI not only facilitates reliable channel acquisition but also significantly reduces the backhaul overhead since only the statistical CSI is shared among the satellites. From the achievable rate analysis, we demonstrate that the achievable rate of the proposed CF-mNTN is higher than that of the conventional cooperative transmission scheme relying on the instantaneous CSI (i.e., cell-free massive MIMO (CF-mMIMO) system). Also, from the extensive simulations on the realistic xG LEO satellite communication environments, we show that CF-mNTN substantially improves the spectral efficiency over the conventional beam-centric systems, particularly for the UEs in the boundaries of satellite footprints.

The key contributions of this paper can be summarized as follows:

- we develop a user-centric cooperative communication framework called CF-mNTN for xG LEO satellite mega-constellation systems;
- we propose a statistical CSI-based data transmission/reception technique and joint satellite clustering and power allocation algorithm; and
- we demonstrate from the achievable rate analysis and extensive simulations that CF-mNTN is very effective in improving the spectral efficiency and coverage.

The rest of this article is organized as in the following. Section II presents the LEO satellite mega-constellation systems and reviews the conventional CF-mMIMO systems and beam-centric systems. Sections III and IV explain the communication protocols of CF-mNTN and user-centric satellite clustering and power allocation algorithm. Section V presents the achievable rate analysis of CF-mNTN. Section VI presents the simulation results. Section VII concludes the paper.

Notations: Random variables are displayed in sans serif, upright fonts; their realizations in serif, italic fonts. Vectors and matrices are denoted by bold lowercase and uppercase letters, respectively. For example, a random variable and its realization are denoted by x and x for scalars, $\mathbf{x}$ and $\boldsymbol{x}$ for vectors, and $\mathbf{X}$ and $\boldsymbol{X}$ for matrices. Sets and random sets are denoted by upright sans serif and calligraphic font, respectively. For example, a random set and its realization are denoted by X and $\mathcal{X}$, respectively. The expectation and variance of a random vector $\mathbf{x}$ are denoted by $\mathbb{E}\{\mathbf{x}\}$ and $\mathbb{V}\{\mathbf{x}\}$, respectively. The covariance between two random vectors $\mathbf{x}$ and $\mathbf{y}$ is denoted by $\mathbb{C}\mathrm{ov}\{\mathbf{x},\mathbf{y}\}$. The m-by-n matrix of zeros is denoted by $\mathbf{0}_{m\times n}$; when $n=1$, the m-dimensional vector of zeros is simply denoted by $\mathbf{0}_m$. The m-by-m identity matrix is denoted by $\boldsymbol{I}_m$. The operators $\mathrm{tr}(\boldsymbol{x})$, $\|\boldsymbol{x}\|_2$, and $\|\boldsymbol{X}\|_{\mathrm{F}}$ denote the trace, the Euclidean norm, and the Frobenius norm, respectively. The operation $\otimes$ denotes the Kronecker product. The transpose, conjugate, and conjugate transpose of $\boldsymbol{X}$ are denoted by $(\cdot)^{\mathrm{T}}$, $(\cdot)^*$, and $(\cdot)^{\mathrm{H}}$, respectively. The real and imaginary parts of a complex number are denoted by $\Re\{\cdot\}$ and $\Im\{\cdot\}$, respectively. The notation $\mathrm{diag}(\cdot)$ represents a diagonal matrix with the arguments being its diagonal elements.

II. LEO Satellite Mega-Constellation Systems

In this section, we present the LEO satellite mega-constellation systems and then review the conventional beam-centric systems and the CF-mMIMO system that performs the joint transmission based on the instantaneous CSI.

A. LEO Satellite Mega-Constellation System Model

We consider a LEO satellite mega-constellation system where L LEO satellites equipped with $N = N_{\mathrm{h}} \times N_{\mathrm{v}}$ uniform planar array (UPA) antennas cooperatively serve K UEs equipped with a single antenna using the same time-frequency resources. The sets of LEO satellites and UEs are denoted as $\mathcal{L} = \{1,2,\ldots,L\}$ and $\mathcal{K} = \{1,2,\ldots,K\}$, respectively. Also, the set of LEO satellites serving the kth UE is denoted as $\mathcal{L}_k \subseteq \mathcal{L}$ and the set of UEs associated with the lth LEO satellite is given by $\mathcal{K}_l = \{k \in \mathcal{K} \mid l \in \mathcal{L}_k\} \subseteq \mathcal{K}$. The LEO satellites are connected to the central node (e.g., MEO or GEO satellites) via an optical backhaul to share satellite and UE positions, statistical CSI, power weights, transmit data, and synchronization and control signal.[1] The 3D position vectors of the lth LEO satellite and the kth UE are $\boldsymbol{p}_l^{\mathrm{sat}} = [p_{l,x}^{\mathrm{sat}}\ p_{l,y}^{\mathrm{sat}}\ p_{l,z}^{\mathrm{sat}}]^{\mathrm{T}}$ and $\boldsymbol{p}_k^{\mathrm{ue}} = [p_{k,x}^{\mathrm{ue}}\ p_{k,y}^{\mathrm{ue}}\ p_{k,z}^{\mathrm{ue}}]^{\mathrm{T}}$, respectively. We assume that both the LEO satellites and the UEs know their positions [35], [36], [37]. Note that the LEO satellite positions can be obtained from the ephemeris data which includes information on the orbital elements and trajectories of the LEO satellites. Also, the UE positions can be obtained by utilizing the global navigation satellite system (GNSS) data and advanced positioning techniques utilizing time-based measurements (e.g., time difference of arrival (TDOA)), Doppler-based measurements (e.g., Doppler shift), and angle-based measurements (e.g., angle of departure (AOD)) [38], [39], [40], [41], [42], [43], [44].

In practical LEO communication systems, one can consider K groups of adjacent UEs instead of K individual UEs. This is because the statistical CSI of adjacent UEs is fairly similar, as their positional differences are negligible compared to the distance between LEO satellites and terrestrial UEs (approximately $1{,}200$ km). For example, the angular resolution (i.e., the smallest angle between two distinct signal sources that an antenna array can distinguish) of a LEO satellite equipped with an $N = 8\times 8$ planar antenna array is $\theta_{\min} = \frac{2}{\sqrt{N}} \approx 14.3^\circ$. This means that adjacent UEs within the off-nadir angular range of radius $\frac{\theta_{\min}}{2} = 7.2^\circ$ can be regarded as a group of UEs sharing the same statistical CSI. In this case, to ensure reliable QoS for these groups of UEs, one can consider a hybrid system architecture where the time-frequency resources are reused across the UE groups and the UEs within the same group are allocated with distinct time-frequency resources.

B. LEO Satellite Channel Model

In NTN, due to the high altitude of satellites, the chance of having a line-of-sight (LOS) link between the satellites and the UEs is much higher compared to terrestrial networks. Based on this observation, we use the non-shadowed Rician fading channel model where the downlink channel vector $\mathbf{h}_{l,k} \in \mathbb{C}^N$ from the lth LEO satellite to the kth UE is expressed as a weighted sum of the LOS and non-line-of-sight (NLOS) components as [45]

$$\mathbf{h}_{l,k} = \sqrt{\frac{\beta_{l,k}}{\kappa_{l,k}+1}}\left(\sqrt{\kappa_{l,k}}\, e^{j2\pi(t\nu_{l,k} - f\tau_{l,k})} + \boldsymbol{\alpha}_{l,k}\right)\boldsymbol{a}(\theta_{l,k},\varphi_{l,k}) \tag{1}$$

where f is the signal frequency, t is the time instant, and $\kappa_{l,k}$ is the Rician K-factor representing the power ratio between

[1] Note that due to the mobility of LEO satellites, a group of LEO satellites connected to a specific GEO satellite can vary over time, which may cause a delay in the statistical CSI acquisition for the GEO satellite. However, since the position errors caused by this handover delay are negligible compared to the LEO satellite communication distance (see Section III-A for detailed discussions), its impact on the satellite clustering and power allocation operation will be marginal.

LOS and NLOS components, $\nu_{l,k}^{\mathrm{sat}} = \frac{f}{c}\frac{d}{dt}\|\boldsymbol{p}_l^{\mathrm{sat}} - \boldsymbol{p}_k^{\mathrm{ue}}\|_2$ is the Doppler shift, $\tau_{l,k}^{\mathrm{sat}} = \frac{1}{c}\|\boldsymbol{p}_l^{\mathrm{sat}} - \boldsymbol{p}_k^{\mathrm{ue}}\|_2$ is the LOS propagation delay, c is the speed of light, and $\alpha_{l,k}$ is the small-scale fading coefficient accounting for the random scattering around the UE. We assume that small-scale fading coefficients are independently and identically distributed (i.i.d.) complex normal random variables (i.e., $\alpha_{l,k} \sim \mathcal{CN}(0,1)$). Also, $\beta_{l,k} = G^{\mathrm{sat}} G^{\mathrm{ue}} L_{l,k}^{\mathrm{free}} L_{l,k}^{\mathrm{abs}}$ is the large-scale fading coefficient accounting for the satellite and UE antenna gains G^{sat} and G^{ue}, the free space path loss $L_{l,k}^{\mathrm{free}} = (\frac{c}{4\pi f \|\boldsymbol{p}_l^{\mathrm{sat}} - \boldsymbol{p}_k^{\mathrm{ue}}\|_2})^2$, and the atmospheric absorption $L_{l,k}^{\mathrm{abs}} = \frac{L_{\mathrm{zenith}}(f)}{\sin\theta_{l,k}}$ where $L_{\mathrm{zenith}}(f)$ is the zenith atmospheric attenuation determined by the satellite altitude [32]. The reference values of $L_{\mathrm{zenith}}(f)$ are given in ITU-R. In addition, $\theta_{l,k}$ and $\varphi_{l,k}$ are the elevation and azimuth AODs of the LOS path, which can be obtained by transforming the relative position vector in the coordinate system of the lth LEO satellite $\tilde{\boldsymbol{p}}_{l,k} = \boldsymbol{R}_y^{-1}(\theta_l^{\mathrm{sat}})\boldsymbol{R}_z^{-1}(\varphi_l^{\mathrm{sat}})(\boldsymbol{p}_k^{\mathrm{ue}} - \boldsymbol{p}_l^{\mathrm{sat}})$ to the spherical coordinate vector. Here, θ_l^{sat} and φ_l^{sat} are elevation and azimuth angles of the normal vector of the lth LEO satellite antenna plane and $\boldsymbol{R}_y(\theta_l^{\mathrm{sat}})$ and $\boldsymbol{R}_z(\varphi_l^{\mathrm{sat}})$ are the y and z-axes rotation matrices, respectively. The corresponding UPA steering vector $\boldsymbol{a}(\theta_{l,k}, \varphi_{l,k}) \in \mathbb{C}^N$ is defined as

$$\boldsymbol{a}(\theta_{l,k}, \varphi_{l,k}) \triangleq \boldsymbol{a}_{\mathrm{h}}(\theta_{l,k}, \varphi_{l,k}) \otimes \boldsymbol{a}_{\mathrm{v}}(\theta_{l,k}) \tag{2}$$

where $\boldsymbol{a}_{\mathrm{h}}(\theta_{l,k}, \varphi_{l,k})$ and $\boldsymbol{a}_{\mathrm{v}}(\theta_{l,k})$ are the horizontal and vertical array steering vectors, respectively, defined as

$$\boldsymbol{a}_{\mathrm{h}}(\theta_{l,k}, \varphi_{l,k}) \triangleq \Big[\, 1 \;\; e^{-j\frac{2\pi f d_{\mathrm{h}}}{c}\sin\theta_{l,k}\cos\varphi_{l,k}} \cdots e^{-j(N_{\mathrm{h}}-1)\frac{2\pi f d_{\mathrm{h}}}{c}\sin\theta_{l,k}\cos\varphi_{l,k}} \Big]^{\mathrm{T}} \tag{3}$$

$$\boldsymbol{a}_{\mathrm{v}}(\theta_{l,k}) \triangleq \Big[\, 1 \;\; e^{-j\frac{2\pi f d_{\mathrm{v}}}{c}\cos\theta_{l,k}} \cdots e^{-j(N_{\mathrm{v}}-1)\frac{2\pi f d_{\mathrm{v}}}{c}\cos\theta_{l,k}} \Big]^{\mathrm{T}} \tag{4}$$

where d_{h} and d_{v} are the horizontal and vertical antenna spacings, respectively.

Note that the same array steering vector $\boldsymbol{a}(\theta_{l,k}, \varphi_{l,k})$ is used for both the LOS and NLOS components of $\mathbf{h}_{l,k}$. This is because the scattering on the ground takes place within a few kilometers around the UEs while the altitudes of the LEO satellites are nearly a thousand kilometers, rendering the angular spread of LEO satellite channel almost negligible [23]. For brevity, we use the following notations.

$$\phi_{l,k} \triangleq 2\pi(t\nu_{l,k} - f\tau_{l,k}) \tag{5}$$

$$v_{l,k} \triangleq \frac{\beta_{l,k}}{\kappa_{l,k}+1} \tag{6}$$

$$\boldsymbol{a}_{l,k} \triangleq \boldsymbol{a}(\theta_{l,k}, \varphi_{l,k})\,. \tag{7}$$

Using these, $\mathbf{h}_{l,k}$ in (1) can be rewritten as

$$\mathbf{h}_{l,k} = \sqrt{v_{l,k}}\left(\sqrt{\kappa_{l,k}}\, e^{j\phi_{l,k}} + \alpha_{l,k}\right)\boldsymbol{a}_{l,k}\,. \tag{8}$$

Among the channel parameters, we categorize the elevation and azimuth AODs $(\theta_{l,k}, \varphi_{l,k})$, the large-scale fading coefficient $\beta_{l,k}$, the Rician K-factor $\kappa_{l,k}$, the Doppler shift $\nu_{l,k}$, and the propagation delay $\tau_{l,k}$ as the statistical CSI. These parameters are primarily determined by the positions of satellites and UEs (i.e., $\boldsymbol{p}_l^{\mathrm{sat}}$ and $\boldsymbol{p}_k^{\mathrm{ue}}$), whereas the small-scale fading coefficient $\alpha_{l,k}$ depends on the randomly varying scatterers (e.g., cars and leaves) around the UEs. Due to this reason, the coherence time of the statistical CSI is typically an order of magnitude longer than that of the path gains [46]. By exploiting these properties, the LEO satellites can directly acquire the statistical CSI from the satellite and UE positions without any pilot transmission and CSI feedback operations.

C. Conventional Beam-Centric and CF-mMIMO Systems

1) Beam-Centric LEO Mega-Constellation Systems: In the traditional beam-centric LEO satellite constellation systems, the LEO satellites employ multiple spot beams, each of which covers a designated terrestrial area [16]. Then the UEs connect to the spot beam providing the maximum received signal power. For instance, the SpaceX's LEO satellites employ 48 spot beams with tessellated hexagonal-shaped footprints and the diameter of each spot beam footprint is around 200 km. While the beam-centric approach might be effective to some extent, it will impose a fundamental limit in the LEO mega-constellation systems due to the frequent handovers among beams and satellites [32], [33]. Since the UE is linked to only one spot beam at a time, the UE has to switch to a different spot beam or satellite when the satellite's position changes, causing significant handover latency and QoS degradation. For example, in the Iridium system, it has been reported that the inter-satellite handovers occur every 10 minutes and the inter-beam handovers happen within every minute.

2) Cell-Free Massive MIMO Systems: In the terrestrial networks, CF-mMIMO system where a group of distributed access points (APs) simultaneously serves UEs has received a great deal of attention recently [47], [48], [49], [50]. This is the opposite concept of traditional cellular system where the network is divided into regional cells (i.e., service areas of APs) and each UE is served only by the AP corresponding to the cell in which the UE is located. In accordance with this trend, there have been some efforts to employ CF-mMIMO approach for NTN [29]. While the CF-mMIMO approach is effective to some extent in terrestrial networks, it might not work well in NTN due to the high mobility and propagation delays of satellites. Specifically, in the CF-mMIMO system, the APs acquire the instantaneous downlink CSI from the uplink pilot signals of UEs and then perform the instantaneous CSI-based downlink precoding. In NTN, however, acquiring the instantaneous CSI at the LEO satellites is highly challenging due to the fast-varying and inherently delayed nature of LEO satellite channel [45]. For example, the coherence time of Ku-band (12)-18 GHz) LEO satellite channel is typically a few milliseconds while that of the terrestrial mmWave channels in the FR1 band (sub-6 GHz) is tens of milliseconds. Moreover, due to the high altitude (500-1, 500 km) of LEO satellites, the coherence time of LEO satellite channel is shorter than the propagation delay (3)-8 ms), meaning that the estimated channel information will be outdated by the time data transmission occurs.

III. Cell-Free Massive Non-Terrestrial Networks

As mentioned, the major issue of the conventional beam-centric systems is the frequent inter-beam and inter-satellite

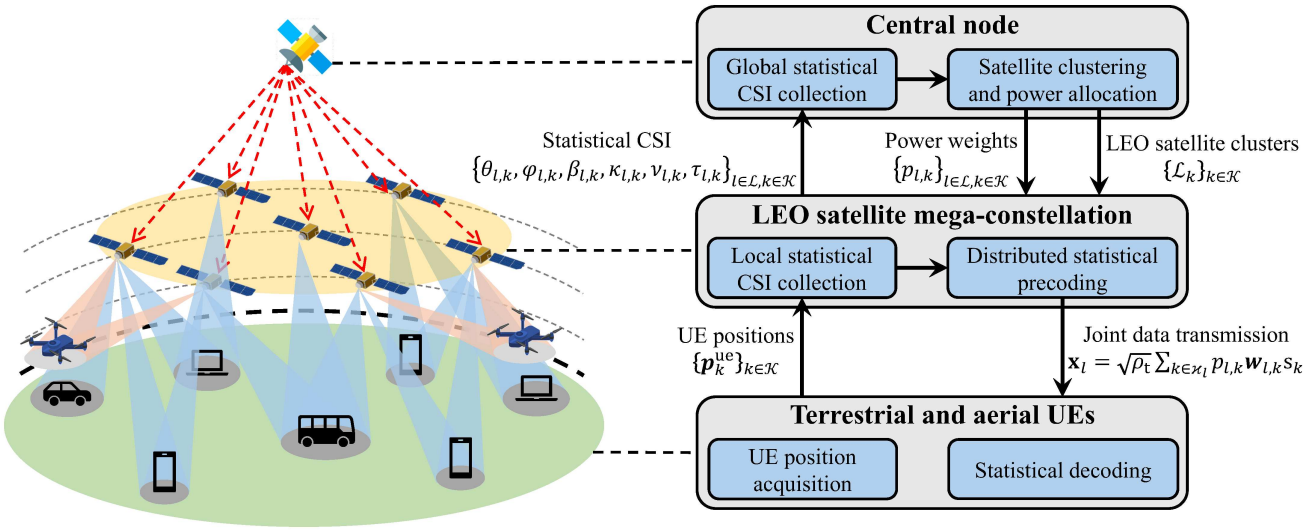

Fig. 2. Overall system structure of CF-mNTN.

handovers caused by the high mobilities of LEO satellites. To address this issue, the proposed CF-mNTN exploits a user-centric approach that chooses a cluster of LEO satellites for each UE and then the satellite cluster cooperatively serves the UE through statistical precoding (see Fig. 2). The key features of CF-mNTN are as in the following.

- **User-centric boundaryless service and full frequency reuse**: In CF-mNTN, the associations between the LEO satellites and UEs are dynamically adjusted according to the wireless environments. In doing so, the inter-beam and inter-satellite handovers can be minimized, thereby achieving seamless connectivity in the xG ground-air-space network. Also, since the LEO satellites serve the UEs using the same time-frequency resources, the spectral efficiency can be enhanced substantially.
- **Statistical CSI-based data transmission and reception**: In CF-mNTN, the downlink data precoding and decoding are performed based on the statistical CSI (e.g., AODs and large-scale fading coefficients). Since the statistical CSI changes more slowly than the instantaneous CSI and is determined primarily by the satellites and UEs positions, the LEO satellites and UEs can accurately acquire them even in the fast-varying NTN.
- **Distributed precoding and cooperative power allocation**: In CF-mNTN, the statistical precoding vectors are determined locally at the LEO satellites while the satellite clusters ans power weights are determined globally at the central node. Since only the statistical CSI, satellite cluster indices, and power weights are shared between the LEO satellites and the central node, the backhaul signaling overhead can be reduced significantly.

In a nutshell, the overall communication protocol of CF-mNTN consists of three major steps (see Fig. 2): 1) the LEO satellites acquire the statistical CSI from the LEO satellites and UEs positions and then send the collected statistical CSI to the central node; 2) the central node determines the satellite clusters and power weights; 3) the LEO satellites jointly transmit the downlink data using the statistical precoding; and 4) the UEs perform the statistical data decoding.

A. Position-Based Statistical CSI Acquisition

In this stage, the LEO satellites first acquire the satellite and UE positions $\{\boldsymbol{p}_l^{\mathrm{sat}}\}_{l\in\mathcal{L}}$ and $\{\boldsymbol{p}_k^{\mathrm{ue}}\}_{k\in\mathcal{K}}$ by exploiting the GNSS data along with the advanced positioning techniques based on time measurements (i.e., TDOA), Doppler-based measurements (e.g., Doppler shift), and angle measurements (i.e., AOD) [51], [52], [53], [54], [55]. Then, using the property that the statistical CSI is a function of the satellite and UE positions, the LEO satellites estimate the statistical CSI of users, i.e., the elevation and azimuth AODs $\theta_{l,k}$ and $\varphi_{l,k}$, the large-scale fading coefficient $\beta_{l,k}$, the Rician K-factor $\kappa_{l,k}$, the Doppler shift $\nu_{l,k}$, and the propagation delay $\tau_{l,k}$. After that, the acquired statistical CSI is sent to the central node through an optical backhaul link to facilitate the satellite cooperation.

Note that the position information of LEO satellites and UEs can be outdated due to signal propagation delay in LEO satellite communications. However, since the position errors caused by this signal propagation delay are negligible compared to the NTN communication distance, the impact of these delays on the statistical CSI is marginal. Specifically, considering that the distances of the LEO-GEO inter-satellite link and the LEO satellite-terrestrial UE link are $D_{\mathrm{sat}} \approx 36{,}000$ km and $D \approx 1{,}200$ km, respectively, the signal propagation delays for these two links are $\tau_{\mathrm{sat}} \approx 120$ ms and $\tau_{\mathrm{ue}} \approx 4$ ms, respectively. If the speeds of the LEO satellite and UE are $v_{\mathrm{sat}} \approx 7.8$ km/s and $v_{\mathrm{ue}} \approx 20$ m/s, respectively, then the LEO satellite and UE position errors are $\Delta r_{\mathrm{sat}} = v_{\mathrm{sat}}\tau_{\mathrm{sat}} \approx 0.94$ km and $\Delta r_{\mathrm{ue}} = v_{\mathrm{ue}}\tau_{\mathrm{ue}} \approx 8 \times 10^{-5}$ km, both of which are negligible compared to D.

B. Downlink Statistical Precoding

After the statistical CSI acquisition, each LEO satellite locally determines the statistical precoding vectors $\{\boldsymbol{w}_{l,k}\}_{l\in\mathcal{L},k\in\mathcal{K}}$ using the acquired statistical CSI $\{\theta_{l,k}, \varphi_{l,k}, \beta_{l,k}, \kappa_{l,k}, \nu_{l,k}, \tau_{l,k}\}_{l\in\mathcal{L},k\in\mathcal{K}}$. In the conventional CF-mMIMO, linear precoding techniques such as maximum ratio transmission (MRT) precoding and zero-forcing (ZF) precoding have been widely used [29], [47]. In CF-mNTN, however, these techniques are not applicable since the LEO

satellites only have the statistical channel information of the UEs. As a remedy, we leverage the observation that the downlink LEO satellite channel vector $\mathbf{h}_{l,k}$ aligns with the LOS array steering vector $\boldsymbol{a}_{l,k}$ (see (8)). This observation implies that we can use the array steering vector to achieve the goals of conventional linear precoding techniques (e.g., channel gain maximization or interference mitigation). Based on this observation, we propose two statistical precoding techniques for CF-mNTN: 1) statistical MRT (sMRT) precoding; and 2) statistical ZF (sZF) precoding.

1) Statistical MRT Precoding: The goal of sMRT precoding technique is to maximize the channel gain $|\mathbf{h}_{l,k}^{\mathrm{H}}\boldsymbol{w}_{l,k}|$. To achieve this goal, we design the sMRT precoding vector $\boldsymbol{w}_{l,k}^{\mathrm{sMRT}} \in \mathbb{C}^N$ from the lth LEO satellite to the kth UE in the form of the array steering vector as

$$\boldsymbol{w}_{l,k}^{\mathrm{sMRT}} \triangleq \frac{1}{\sqrt{N}} e^{j\phi_{l,k}} \boldsymbol{a}_{l,k}\,. \tag{9}$$

Note that $e^{j\phi_{l,k}} = e^{j2\pi(t\nu_{l,k} - f\tau_{l,k})}$ is used for the compensation of the Doppler shift and propagation delay. Since $\boldsymbol{w}_{l,k}^{\mathrm{sMRT}}$ is parallel to $\mathbf{h}_{l,k}$, it maximizes the channel gain as

$$\left|\mathbf{h}_{l,k}^{\mathrm{H}}\boldsymbol{w}_{l,k}^{\mathrm{sMRT}}\right| = \left|\mathbf{h}_{l,k}^{\mathrm{H}}\frac{\mathbf{h}_{l,k}}{\|\mathbf{h}_{l,k}\|_2}\right| = \|\mathbf{h}_{l,k}\|_2\,. \tag{10}$$

2) Statistical ZF Precoding: Similar to the conventional ZF precoding, the goal of sZF precoding is to mitigate inter-user interference (IUI) (i.e., $\left|\mathbf{h}_{l,j}^{\mathrm{H}}\boldsymbol{w}_{l,k}\right| = 0$ if $j \neq k$). To do so, the precoding vector of each UE should be selected from the intersection of the null-spaces of the channel vectors of other UEs. Note that since $\boldsymbol{h}_{l,j}$ and $\boldsymbol{a}_{l,j}$ are parallel, their null-spaces are the same. Using this property, we design the sZF precoding vector $\boldsymbol{w}_{l,k}^{\mathrm{sZF}} \in \mathbb{C}^N$ as

$$\boldsymbol{w}_{l,k}^{\mathrm{sZF}} \triangleq e^{j\phi_{l,k}} \frac{\boldsymbol{A}_l\left(\boldsymbol{A}_l^{\mathrm{H}}\boldsymbol{A}_l\right)^{-1}\boldsymbol{e}_k}{\|\boldsymbol{A}_l\left(\boldsymbol{A}_l^{\mathrm{H}}\boldsymbol{A}_l\right)^{-1}\boldsymbol{e}_k\|_2} \tag{11}$$

where $\boldsymbol{A}_l = \left[\boldsymbol{a}_{l,1}\,\boldsymbol{a}_{l,2}\cdots\boldsymbol{a}_{l,K}\right] \in \mathbb{C}^{N\times K}$ is the array steering matrix of the lth LEO satellite and $\boldsymbol{e}_k \in \mathbb{R}^K$ is a $K \times 1$ vector whose kth element is 1 and all other elements are 0. One can see that $\boldsymbol{w}_{l,k}^{\mathrm{sZF}}$ effectively suppresses IUI as

$$\left|\mathbf{h}_{l,j}^{\mathrm{H}}\boldsymbol{w}_{l,k}^{\mathrm{sZF}}\right| = \frac{\|\mathbf{h}_{l,j}\|_2\left|\boldsymbol{a}_{l,j}^{\mathrm{H}}\boldsymbol{A}_l\left(\boldsymbol{A}_l^{\mathrm{H}}\boldsymbol{A}_l\right)^{-1}\boldsymbol{e}_k\right|}{N\|\boldsymbol{A}_l\left(\boldsymbol{A}_l^{\mathrm{H}}\boldsymbol{A}_l\right)^{-1}\boldsymbol{e}_k\|_2} = 0\,. \tag{12}$$

C. Downlink Data Transmission and Statistical Decoding

Once the downlink precoding vectors are determined, the LEO satellites jointly transmit the precoded data and then the UEs decode the data using the statistical CSI. The transmit signal $\mathbf{x}_l \in \mathbb{C}^N$ of the lth LEO satellite is given by

$$\mathbf{x}_l = \sqrt{\rho_{\mathrm{t}}}\sum_{k\in\mathcal{K}_l} p_{l,k}\boldsymbol{w}_{l,k}\mathsf{s}_k \tag{13}$$

where ρ_{t} is the satellite transmission power, $\boldsymbol{w}_{l,k} \in \mathbb{C}^N$ is the downlink statistical precoding vector from the lth LEO satellite to the kth UE such that $\|\boldsymbol{w}_{l,k}\|_2 = 1$, $p_{l,k} \geqslant 0$ is the power weight, and $\mathsf{s}_k \sim \mathcal{CN}(0,1)$ is the data symbol for the kth UE. Note that the power of $\mathbf{x}_l$ is bounded by the LEO satellite transmission power ρ_{t} as

$$\mathbb{E}\left\{\|\mathbf{x}_l\|_2^2\right\} = \rho_{\mathrm{t}}\sum_{k\in\mathcal{K}_l} p_{l,k}^2 \leqslant \rho_{\mathrm{t}}\,. \tag{14}$$

Then the received data signal $\mathsf{y}_k \in \mathbb{C}$ of the kth UE is

$$\begin{aligned}\mathsf{y}_k &= \sum_{l=1}^{L}\mathbf{h}_{l,k}^{\mathrm{H}}\mathbf{x}_l + \mathsf{n}_k &(15)\\ &= \sqrt{\rho_{\mathrm{t}}}\sum_{l\in\mathcal{L}_k} p_{l,k}\mathbf{h}_{l,k}^{\mathrm{H}}\boldsymbol{w}_{l,k}\mathsf{s}_k \\ &\quad + \sqrt{\rho_{\mathrm{t}}}\sum_{j\neq k}\sum_{l\in\mathcal{L}_j} p_{l,j}\mathbf{h}_{l,k}^{\mathrm{H}}\boldsymbol{w}_{l,j}\mathsf{s}_j + \mathsf{n}_k &(16)\end{aligned}$$

where (16) is from $\sum_{l=1}^{L}\sum_{j\in\mathcal{K}_l} a_{l,j} = \sum_{j=1}^{K}\sum_{l\in\mathcal{L}_j} a_{l,j}$ and $\mathsf{n}_k \sim \mathcal{CN}(0,\sigma_{\mathrm{n}}^2)$ is the additive Gaussian noise. Note that the first and second terms represent the effective channel gain and IUI, respectively. In traditional terrestrial networks, to facilitate the acquisition of effective channel gain at UE, the AP transmits the precoded downlink pilot signal (i.e., demodulation reference signals (DMRS) in 5G NR) to the UE. In NTN, however, the estimated effective channel gain might be significantly outdated due to the short channel coherence time and the large propagation delay, causing a severe degradation in the decoding performance.

To handle this issue, we exploit the property that the effective channel gain combined from multiple LEO satellites tends to its mean value (i.e., $\sum_{l\in\mathcal{L}_k} p_{l,k}\mathbf{h}_{l,k}^{\mathrm{H}}\boldsymbol{w}_{l,k} \to \mathbb{E}\{\sum_{l\in\mathcal{L}_k} p_{l,k}\mathbf{h}_{l,k}^{\mathrm{H}}\boldsymbol{w}_{l,k}\}$). Based on this channel hardening effect, in CF-mNTN, the UEs extract the expectation of the effective channel gain from the received signal using only the statistical CSI. Specifically, y_k in (16) can be rewritten as

$$\mathsf{y}_k = \gamma_k^{\mathrm{ds}}\mathsf{s}_k + \boldsymbol{\gamma}_k^{\mathrm{bu}}\mathsf{s}_k + \sum_{j\neq k}\boldsymbol{\gamma}_{k,j}^{\mathrm{ui}}\mathsf{s}_j + \mathsf{n}_k \tag{17}$$

where γ_k^{ds}, $\boldsymbol{\gamma}_k^{\mathrm{bu}}$, and $\boldsymbol{\gamma}_{k,j}^{\mathrm{ui}}$ are the desired signal term, the beamforming uncertainty term, and the IUI term, defined as

$$\gamma_k^{\mathrm{ds}} \triangleq \mathbb{E}\Big\{\sqrt{\rho_{\mathrm{t}}}\sum_{l\in\mathcal{L}_k} p_{l,k}\mathbf{h}_{l,k}^{\mathrm{H}}\boldsymbol{w}_{l,k}\Big\} \tag{18}$$

$$\boldsymbol{\gamma}_k^{\mathrm{bu}} \triangleq \sqrt{\rho_{\mathrm{t}}}\sum_{l\in\mathcal{L}_k} p_{l,k}\mathbf{h}_{l,k}^{\mathrm{H}}\boldsymbol{w}_{l,k} - \mathbb{E}\Big\{\sqrt{\rho_{\mathrm{t}}}\sum_{l\in\mathcal{L}_k} p_{l,k}\mathbf{h}_{l,k}^{\mathrm{H}}\boldsymbol{w}_{l,k}\Big\} \tag{19}$$

$$\boldsymbol{\gamma}_{k,j}^{\mathrm{ui}} \triangleq \sqrt{\rho_{\mathrm{t}}}\sum_{l\in\mathcal{L}_j} p_{l,j}\mathbf{h}_{l,k}^{\mathrm{H}}\boldsymbol{w}_{l,j}\,. \tag{20}$$

By treating $\boldsymbol{\gamma}_k^{\mathrm{bu}}$, $\boldsymbol{\gamma}_{k,j}^{\mathrm{ui}}$, and n_k as effective noise and using the rate approximation in [56, Lemma 1], we obtain the downlink ergodic achievable rate R_k^{CFmNTN} of the kth UE as

$$R_k^{\mathrm{CFmNTN}} = \log_2\left(1 + \frac{|\gamma_k^{\mathrm{ds}}|^2}{\mathbb{E}\left\{|\boldsymbol{\gamma}_k^{\mathrm{bu}}|^2\right\} + \sum_{j\neq k}\mathbb{E}\left\{|\boldsymbol{\gamma}_{k,j}^{\mathrm{ui}}|^2\right\} + \sigma_{\mathrm{n}}^2}\right). \tag{21}$$

The following theorem provides a closed-form expression of R_k^{CFmNTN}.

Theorem 1: The downlink achievable rate R_k^{CFmNTN} of the kth UE of CF-mNTN using the sMRT and sZF precodings is expressed in (22), as shown at the bottom of the next page. □

Proof: See Appendix A. ⊠

From (22), one can see that R_k^{CFmNTN} is a function of the satellite cluster indices $\{\mathcal{L}_k\}_{k\in\mathcal{K}}$, the power

weights $\{p_{l,k}\}_{l\in\mathcal{L},k\in\mathcal{K}}$, and the statistical CSI $\{\theta_{l,k},\varphi_{l,k},\beta_{l,k},\kappa_{l,k},\nu_{l,k},\tau_{l,k}\}_{l\in\mathcal{L},k\in\mathcal{K}}$. Hence, by utilizing the statistical CSI collected from the LEO satellites, the central node can determine the LEO satellite clusters and the power weights maximizing the sum-rate.

IV. User-Centric LEO Satellite Clustering and Cooperative Power Allocation

In this section, we present a joint user-centric LEO satellite clustering and cooperative power allocation technique for CF-mNTN. Specifically, the proposed technique determines the optimal LEO satellite clusters $\{\mathcal{L}_k\}_{k\in\mathcal{K}}$ and the power weights $\{p_{l,k}\}_{l\in\mathcal{L},k\in\mathcal{K}}$ maximizing the minimum achievable rate of UEs. In doing so, one can ensure a uniformly good QoS for all UEs within the coverage area. The corresponding optimization problem can be formulated as the max-min problem $\mathscr{P}_1$ as[2]

$$\mathscr{P}_1: \underset{\{\mathcal{L}_k,p_{l,k}\}_{l\in\mathcal{L},k\in\mathcal{K}}}{\text{maximize}} \quad \min_{k\in\mathcal{K}} R_k^{\text{CFmNTN}} \tag{23a}$$

$$\text{subject to} \quad |\mathcal{K}_l| \leqslant K_{\max} \qquad \forall\, l\in\mathcal{L} \tag{23b}$$

$$\sum_{k\in\mathcal{K}_l} p_{l,k}^2 \leqslant 1 \qquad \forall\, l\in\mathcal{L} \tag{23c}$$

$$p_{l,k} \geqslant 0 \qquad \forall\, l\in\mathcal{L},\, k\in\mathcal{K} \tag{23d}$$

where $\mathcal{K}_l = \{k \in \mathcal{K} \mid l \in \mathcal{L}_k\}$ is the set of UEs associated with the lth LEO satellite. Also, (23b) represents the constraint that the total number of UEs associated to each LEO satellite is bounded by $K_{\max}$ due to the limited number of RF chains and (23c) and (23d) represent the transmit power constraint.

Since the downlink achievable rate is a logarithmic function of the fractional function (see (22)), $\mathscr{P}_1$ is a nonconvex combinatorial optimization problem in which an exhaustive search is needed to find out the optimal solution. In the LEO satellite mega-constellation systems, however, it is computationally burdensome to search every possible satellite association due to the large number of satellites. For example, when the numbers of LEO satellites, terrestrial UEs, and serving satellites are $L = 10$, $K = 5$, and $K_{\max} = 5$, respectively, the number of possible satellite associations is $\binom{10}{5}^5 \approx 10^{12}$.

[2]In practical scenarios where the number of UEs connected to the LEO satellite network changes dynamically, we redefine K as the maximum number of UEs that the LEO satellite network can simultaneously support and define the set of UEs that are actually connected to the LEO satellite network as $\mathcal{K}_{\text{c}} \subseteq \mathcal{K}$. Note that the statistical CSI and the power weights for the inactive UEs in $\mathcal{K}\setminus\mathcal{K}_{\text{c}}$ are set to zero. After that, we modify the objective function of $\mathscr{P}_1$ from $\min_{k\in\mathcal{K}} R_k^{\text{CFmNTN}}$ to $\min_{k\in\mathcal{K}_{\text{c}}} R_k^{\text{CFmNTN}}$ so that only the data rates of connected UEs in $\mathcal{K}_{\text{c}}$ are considered. By doing so, we can effectively cover the scenarios with different number of UEs.

A. Sparse Recovery Problem Formulation

To find out a tractable solution of $\mathscr{P}_1$, we recast the LEO satellite clustering problem to the sparse recovery problem where the indices of serving LEO satellites are mapped to the indices of the nonzero elements (i.e., support) of the sparse power weight vectors. In doing so, we can convert $\mathscr{P}_1$ to the sparse optimization problem, for which the principle of sparse recovery can be applied [57], [58]. To be specific, the sparse power weight vector of the kth UE combined for all LEO satellites within the constellation is defined as $\tilde{\boldsymbol{p}}_k = [\,\tilde{p}_{1,k}\,\tilde{p}_{2,k}\,\cdots\,\tilde{p}_{L,k}\,]^{\text{T}} \in \mathbb{R}^L$ such that

$$\tilde{p}_{l,k} \triangleq \begin{cases} p_{l,k} & \text{if } l\in\mathcal{L}_k \\ 0 & \text{otherwise}. \end{cases} \tag{24}$$

Then the LEO satellite cluster $\mathcal{L}_k$ can be expressed as the set of nonzero elements of $\tilde{\boldsymbol{p}}_k$ as

$$\mathcal{L}_k = \left\{ l\in\mathcal{L} \;\middle|\; \mathbb{1}_{\mathbb{R}^+}(\tilde{p}_{l,k}) = 1 \right\} \tag{25}$$

where $\mathbb{1}_{\mathbb{R}^+}(x)$ is the indicator function such that $\mathbb{1}_{\mathbb{R}^+}(x) = 1$ if $x\in\mathbb{R}^+$ (i.e., $x>0$) and $\mathbb{1}_{\mathbb{R}^+}(x) = 0$ otherwise. Similarly, the cluster size constraint (23b) can be equivalently converted to the sparsity constraint as

$$|\mathcal{K}_l| \leqslant K_{\max} \iff \sum_{k=1}^{K} \mathbb{1}_{\mathbb{R}^+}(\tilde{p}_{l,k}) \leqslant K_{\max}. \tag{26}$$

Also, by defining the coefficient vectors and matrices, R_k^{CFmNTN} in (22) can be rewritten as

$$R_k^{\text{CFmNTN}} = \log_2\left(1 + \frac{\left(\boldsymbol{b}_k^{\text{T}}\tilde{\boldsymbol{p}}_k\right)^2}{\sum_{j=1}^{K}\|\boldsymbol{C}_{k,j}\tilde{\boldsymbol{p}}_k\|_2^2 + \sum_{j\neq k}\|\boldsymbol{D}_{k,j}\tilde{\boldsymbol{p}}_j\|_2^2 + \sigma_{\text{n}}^2}\right) \tag{27}$$

where $\boldsymbol{b}_k \triangleq [\,b_{1,k}\,b_{2,k}\,\cdots\,b_{L,k}\,]^{\text{T}} \in \mathbb{R}^L$, $\boldsymbol{C}_k \triangleq \text{diag}(c_{1,k},c_{2,k},\cdots,c_{L,k}) \in \mathbb{R}^{L\times L}$, and $\boldsymbol{D}_{k,j} \triangleq \begin{bmatrix} \Re\{d_{1,k,j}\} & \Re\{d_{2,k,j}\} & \cdots & \Re\{d_{L,k,j}\} \\ \Im\{d_{1,k,j}\} & \Im\{d_{2,k,j}\} & \cdots & \Im\{d_{L,k,j}\} \end{bmatrix} \in \mathbb{R}^{2\times L}$ are defined as

$$b_{l,k} \triangleq \begin{cases} \sqrt{\rho_{\text{t}} N \kappa_{l,k}\upsilon_{l,k}} & \text{sMRT precoding} \\ \sqrt{\rho_{\text{t}}\kappa_{l,k}\upsilon_{l,k}}\,\|\boldsymbol{A}_l\,(\boldsymbol{A}_l^{\text{H}}\boldsymbol{A}_l)^{-1}\boldsymbol{e}_k\|_2^{-1} & \text{sZF precoding} \end{cases}$$

$$c_{l,k} \triangleq \begin{cases} \sqrt{\dfrac{\rho_{\text{t}}}{N}\upsilon_{l,k}}\,\left|\boldsymbol{a}_{l,k}^{\text{H}}\boldsymbol{a}_{l,j}\right| & \text{sMRT precoding} \\ \sqrt{\rho_{\text{t}}\upsilon_{l,k}}\,\|\boldsymbol{A}_l\,(\boldsymbol{A}_l^{\text{H}}\boldsymbol{A}_l)^{-1}\boldsymbol{e}_k\|_2^{-1} & \text{sZF precoding} \end{cases}$$

$$d_{l,k,j} \triangleq \begin{cases} \sqrt{\dfrac{\rho_{\text{t}}}{N}\kappa_{l,k}\upsilon_{l,k}}\,e^{j(\phi_{l,j}-\phi_{l,k})}\boldsymbol{a}_{l,k}^{\text{H}}\boldsymbol{a}_{l,j} & \text{sMRT precoding} \\ 0 & \text{sZF precoding}. \end{cases} \tag{28}$$

$$R_k^{\text{CFmNTN}} = \begin{cases} \log_2\left(1 + \dfrac{\rho_{\text{t}} N\left(\sum_{l\in\mathcal{L}_k} p_{l,k}\sqrt{\kappa_{l,k}\upsilon_{l,k}}\right)^2}{\frac{\rho_{\text{t}}}{N}\sum_{j=1}^{K}\sum_{l\in\mathcal{L}_j} p_{l,j}^2\upsilon_{l,k}|\boldsymbol{a}_{l,k}^{\text{H}}\boldsymbol{a}_{l,j}|^2 + \frac{\rho_{\text{t}}}{N}\sum_{j\neq k}\left|\sum_{l\in\mathcal{L}_j} p_{l,j}e^{j(\phi_{l,j}-\phi_{l,k})}\sqrt{\kappa_{l,k}\upsilon_{l,k}}\,\boldsymbol{a}_{l,k}^{\text{H}}\boldsymbol{a}_{l,j}\right|^2 + \sigma_{\text{n}}^2}\right) \\ \qquad\qquad \text{sMRT precoding} \\ \log_2\left(1 + \dfrac{\rho_{\text{t}}\left(\sum_{l\in\mathcal{L}_k} p_{l,k}\sqrt{\kappa_{l,k}\upsilon_{l,k}}\|\boldsymbol{A}_l\,(\boldsymbol{A}_l^{\text{H}}\boldsymbol{A}_l)^{-1}\boldsymbol{e}_k\|_2^{-1}\right)^2}{\rho_{\text{t}}\sum_{l\in\mathcal{L}_k} p_{l,k}^2\upsilon_{l,k}\|\boldsymbol{A}_l\,(\boldsymbol{A}_l^{\text{H}}\boldsymbol{A}_l)^{-1}\boldsymbol{e}_k\|_2^{-2} + \sigma_{\text{n}}^2}\right) \\ \qquad\qquad \text{sZF precoding}. \end{cases} \tag{22}$$

Finally, by substituting (24)-(28) into (23) and leveraging the fact that maximizing the minimum achievable rate is equivalent to maximizing the minimum signal-to-interference-plus-noise ratio (SINR), we obtain the sparse recovery problem:

$$\mathscr{P}_2: \underset{t,\{\tilde{\boldsymbol{p}}_k\}_{k\in\mathcal{K}}}{\text{maximize}} \quad t \tag{29a}$$

$$\text{subject to} \quad \frac{\left(\boldsymbol{b}_k^{\mathrm{T}}\tilde{\boldsymbol{p}}_k\right)^2}{\sum_{j=1}^{K}\|\boldsymbol{C}_{k,j}\tilde{\boldsymbol{p}}_k\|_2^2+\sum_{j\neq k}\|\boldsymbol{D}_{k,j}\tilde{\boldsymbol{p}}_j\|_2^2+\sigma_{\mathrm{n}}^2} \geqslant t \qquad \forall k\in\mathcal{K} \tag{29b}$$

$$\sum_{k=1}^{K}\mathbb{1}_{\mathbb{R}^+}(\tilde{p}_{l,k}) \leqslant K_{\max} \qquad \forall l\in\mathcal{L} \tag{29c}$$

$$\sum_{k=1}^{K}\tilde{p}_{l,k}^2 \leqslant 1 \qquad \forall l\in\mathcal{L} \tag{29d}$$

$$\tilde{p}_{l,k} \geqslant 0 \qquad \forall l\in\mathcal{L},\, k\in\mathcal{K} \tag{29e}$$

where $t=\min_{k\in\mathcal{K}}\mathrm{SINR}_k$ is an auxiliary variable.

The reformulated problem $\mathscr{P}_2$ is more tractable than the original problem $\mathscr{P}_1$ since we only have to determine the sparse power weight vector. Unfortunately, it is still not easy to find out the optimal solution of $\mathscr{P}_2$ due to the nonconvexity of the sparsity constraint (29c) and the quadratic fractional SINR constraint (29b). To handle these constraints, we employ two effective strategies: 1) reweighted ℓ_2-norm approximation that transforms the sparsity constraint into the weighted ℓ_2-norm constraint [59] and 2) successive convex approximation (SCA) that approximates the SINR function to a linear function by using the first-order Taylor expansion [60]. Using these, we reformulate $\mathscr{P}_2$ to a convex second-order cone program (SOCP) in which the global optimal solution can be obtained via convex optimization solvers (e.g., SDPT3 and SeDuMi). After solving the reformulated SOCP problem, we update the ℓ_2-norm approximation weights and then repeat these processes until (29c) is satisfied.

B. Reweighted ℓ_2-Norm Approximation

The essence of reweighted ℓ_2-norm approximation is to substitute the indicator function $\mathbb{1}_{\mathbb{R}^+}(\tilde{p}_{l,k})$ with the weighted square function $\omega_{l,k}|\tilde{p}_{l,k}|^2$ where $\omega_{l,k}$ is the ℓ_2-norm approximation weight. By assigning larger approximation weights to the smaller power weights and iteratively updating the approximation weights, this method effectively penalizes these smaller power weights, driving them closer to zero. In doing so, one can promote the sparsity of the power weight vector.

To do so, we set $\omega_{l,k}$ to be inversely proportional to the power weight $\tilde{p}_{l,k}^{\mathrm{prev}}$ obtained in the previous iteration as

$$\omega_{l,k}=\frac{1}{(\tilde{p}_{l,k}^{\mathrm{prev}})^2+\epsilon^{-1}} \tag{30}$$

where $\epsilon>0$ is a regularization factor. By using $\omega_{l,k}$, the sparsity of the power weight vector can be approximated as

$$\sum_{k=1}^{K}\mathbb{1}_{\mathbb{R}^+}(\tilde{p}_{l,k}) \approx \sum_{k=1}^{K}\omega_{l,k}\tilde{p}_{l,k}^2\,. \tag{31}$$

By exploiting the reweighted ℓ_2-norm approximation, we solve $\tilde{\mathscr{P}}$ in an alternating fashion: 1) fix $\{\tilde{\boldsymbol{p}}_k\}_{k\in\mathcal{K}}$ and update $\{\omega_{l,k}\}_{l\in\mathcal{L},k\in\mathcal{K}}$ using (30); and 2) fix $\{\omega_{l,k}\}_{l\in\mathcal{L},k\in\mathcal{K}}$ and solve the reduced problem $\mathscr{P}_3$ given by

$$\mathscr{P}_3: \underset{t,\{\tilde{\boldsymbol{p}}_k\}_{k\in\mathcal{K}}}{\text{maximize}} \quad t \tag{32a}$$

$$\text{subject to} \quad \frac{\left(\boldsymbol{b}_k^{\mathrm{T}}\tilde{\boldsymbol{p}}_k\right)^2}{\sum_{j=1}^{K}\|\boldsymbol{C}_{k,j}\tilde{\boldsymbol{p}}_k\|_2^2+\sum_{j\neq k}\|\boldsymbol{D}_{k,j}\tilde{\boldsymbol{p}}_j\|_2^2+\sigma_{\mathrm{n}}^2} \geqslant t \qquad \forall k\in\mathcal{K} \tag{32b}$$

$$\sum_{k=1}^{K}\omega_{l,k}\tilde{p}_{l,k}^2 \leqslant K_{\max} \qquad \forall l\in\mathcal{L} \tag{32c}$$

$$\sum_{k=1}^{K}\tilde{p}_{l,k}^2 \leqslant 1 \qquad \forall l\in\mathcal{L} \tag{32d}$$

$$\tilde{p}_{l,k} \geqslant 0 \qquad \forall l\in\mathcal{L},\, k\in\mathcal{K}\,. \tag{32e}$$

Although the sparsity constraint (29c) is replaced by the convex quadratic constraint (32c), $\mathscr{P}_3$ is still a nonconvex problem due to the quadratic fractional SINR constraint (32b).

C. Successive Convex Approximation-Based Power Allocation

Next, we describe how to solve $\mathscr{P}_3$ using SCA. SCA is a linear approximation technique based on the first-order Taylor expansion. In our work, we employ SCA to approximate the quadratic fractional function $f(\tilde{\boldsymbol{p}}_k,t)$ defined as

$$f(\tilde{\boldsymbol{p}}_k,t) \triangleq \frac{\left(\boldsymbol{b}_k^{\mathrm{T}}\tilde{\boldsymbol{p}}_k\right)^2}{t}\,. \tag{33}$$

Note that $f(\tilde{\boldsymbol{p}}_k,t)$ is a convex function of $\tilde{\boldsymbol{p}}_k$ and t. Using $f(\tilde{\boldsymbol{p}}_k,t)$, the SINR constraint (32b) can be rewritten as

$$f(\tilde{\boldsymbol{p}}_k,t) \geqslant \sum_{j=1}^{K}\|\boldsymbol{C}_{k,j}\tilde{\boldsymbol{p}}_k\|_2^2+\sum_{j\neq k}\|\boldsymbol{D}_{k,j}\tilde{\boldsymbol{p}}_j\|_2^2+\sigma_{\mathrm{n}}^2 \qquad \forall k\in\mathcal{K}\,. \tag{34}$$

Then, for given $(\tilde{\boldsymbol{p}}_k^{\mathrm{prev}},t^{\mathrm{prev}})$ obtained at the previous iteration, the first-order Taylor expansion $F(\tilde{\boldsymbol{p}}_k,t\mid\tilde{\boldsymbol{p}}_k^{\mathrm{prev}},t^{\mathrm{prev}})$ of $f(\tilde{\boldsymbol{p}}_k,t)$ is given by

$$\begin{aligned}F(\tilde{\boldsymbol{p}}_k,t\mid\tilde{\boldsymbol{p}}_k^{\mathrm{prev}},t^{\mathrm{prev}}) &\triangleq f(\tilde{\boldsymbol{p}}_k,t)+\nabla_{\tilde{\boldsymbol{p}}_k}f(\tilde{\boldsymbol{p}}_k^{\mathrm{prev}},t^{\mathrm{prev}})^{\mathrm{T}}(\tilde{\boldsymbol{p}}_k-\tilde{\boldsymbol{p}}_k^{\mathrm{prev}})\\ &\quad+\partial_t f(\tilde{\boldsymbol{p}}_k^{\mathrm{prev}},t^{\mathrm{prev}})(t-t^{\mathrm{prev}}) \qquad (35)\\ &=\frac{(\tilde{\boldsymbol{p}}_k^{\mathrm{prev}})^{\mathrm{T}}\boldsymbol{b}_k\boldsymbol{b}_k^{\mathrm{T}}(2t^{\mathrm{prev}}\tilde{\boldsymbol{p}}_k-t\tilde{\boldsymbol{p}}_k^{\mathrm{prev}})}{(t^{\mathrm{prev}})^2}\,. \qquad (36)\end{aligned}$$

Since $f(\tilde{\boldsymbol{p}}_k,t)$ is convex, $f(\tilde{\boldsymbol{p}}_k,t)\geqslant F(\tilde{\boldsymbol{p}}_k,t\mid\tilde{\boldsymbol{p}}_k^{\mathrm{prev}},t^{\mathrm{prev}})$, meaning that $(\tilde{\boldsymbol{p}}_k,t)$ satisfying the approximated SINR constraint using $F(\tilde{\boldsymbol{p}}_k,t\mid\tilde{\boldsymbol{p}}_k^{\mathrm{prev}},t^{\mathrm{prev}})$ will also satisfy the original SINR constraint (34).

By substituting $f(\tilde{\boldsymbol{p}}_k,t)$ with $F(\tilde{\boldsymbol{p}}_k,t\mid\tilde{\boldsymbol{p}}_k^{\mathrm{prev}},t^{\mathrm{prev}})$, we obtain the modified problem $\mathscr{P}_4$ as

$$\mathscr{P}_4: \underset{t,\{\tilde{\boldsymbol{p}}_k\}_{k\in\mathcal{K}}}{\text{maximize}} \quad t \tag{37a}$$

$$\text{subject to} \quad \frac{(\tilde{\boldsymbol{p}}_k^{\mathrm{prev}})^{\mathrm{T}}\boldsymbol{b}_k\boldsymbol{b}_k^{\mathrm{T}}(2t^{\mathrm{prev}}\tilde{\boldsymbol{p}}_k-t\tilde{\boldsymbol{p}}_k^{\mathrm{prev}})}{(t^{\mathrm{prev}})^2} \geqslant \sum_{j=1}^{K}\|\boldsymbol{C}_{k,j}\tilde{\boldsymbol{p}}_k\|_2^2+\sum_{j\neq k}\|\boldsymbol{D}_{k,j}\tilde{\boldsymbol{p}}_j\|_2^2+\sigma_{\mathrm{n}}^2 \qquad \forall k\in\mathcal{K} \tag{37b}$$

$$\sum_{k=1}^{K}\omega_{l,k}\tilde{p}_{l,k}^2 \leqslant K_{\max} \qquad \forall l\in\mathcal{L} \tag{37c}$$

$$\sum_{k=1}^{K}\tilde{p}_{l,k}^2 \leqslant 1 \qquad \forall l\in\mathcal{L} \tag{37d}$$

$$\tilde{p}_{l,k} \geqslant 0 \qquad \forall l\in\mathcal{L},\, k\in\mathcal{K}\,. \tag{37e}$$

Algorithm 1 User-Centric LEO Satellite Clustering and Cooperative Power Allocation Algorithm

Input: Statistical CSI $\{\theta_{l,k}, \varphi_{l,k}, \beta_{l,k}, \kappa_{l,k}, \nu_{l,k}, \tau_{l,k}\}_{l\in\mathcal{L},k\in\mathcal{K}}$ satellite transmission power ρ_{t}, maximum number of UEs associated to LEO satellite $K_{\max}$, regularization factor ϵ

Initialize:

Compute $\{\boldsymbol{b}_k, \boldsymbol{C}_{k,j}, \boldsymbol{D}_{k,j}\}_{k,j\in\mathcal{K}}$ using (28) $\quad \forall k,j \in \mathcal{K}$

$\omega_{l,k} = 1 \quad \forall l \in \mathcal{L},\ k \in \mathcal{K}$

while the sparsity constraint (29c) is not satisfied **do**

$\tilde{\boldsymbol{p}}_k^{\mathrm{prev}} = \mathbf{0}_L,\ t^{\mathrm{prev}} = 0 \quad \forall k \in \mathcal{K}$

while $\{\tilde{\boldsymbol{p}}_k\}_{k\in\mathcal{K}}$ do not converge **do**

Solve $\mathscr{P}_4$ via SOCP solver

$\tilde{\boldsymbol{p}}_k^{\mathrm{prev}} = \tilde{\boldsymbol{p}}_k,\ t^{\mathrm{prev}} = t \quad \forall k \in \mathcal{K}$

end while

$\tilde{\boldsymbol{p}}_k^{\mathrm{prev}} = \tilde{\boldsymbol{p}}_k \quad \forall k \in \mathcal{K}$

$\omega_{l,k} = \frac{1}{(\tilde{p}_{l,k}^{\mathrm{prev}})^2+\epsilon^{-1}} \quad \forall l \in \mathcal{L},\ k \in \mathcal{K}$

end while

$\mathcal{L}_k = \{l \in \mathcal{L} \mid \mathbb{1}_{\mathbb{R}^+}(\tilde{p}_{l,k}) = 1\} \quad \forall k \in \mathcal{K}$

$p_{l,k} = \tilde{p}_{l,k} \quad \forall l \in \mathcal{L}_k,\ k \in \mathcal{K}$

Output: $\{\mathcal{L}_k\}_{k\in\mathcal{K}}$, $\{p_{l,k}\}_{l\in\mathcal{L}_k,k\in\mathcal{K}}$

Note that the constraints (37b)-(37d) of $\mathscr{P}_4$ can be reformulated as second-order cone constraints in a form of $\|\boldsymbol{A}\boldsymbol{x} + \boldsymbol{b}\|_2 \leqslant \boldsymbol{c}^{\mathrm{T}}\boldsymbol{x} + d$ [61]. This, together with the fact that the objective function (37a) is a linear function of t, characterizes $\mathscr{P}_4$ as a convex SOCP problem. Thus, by using the convex optimization solver (e.g., SDPT3), we can obtain the optimal solution $(t^{\mathrm{opt}}, \{\tilde{\boldsymbol{p}}_k^{\mathrm{opt}}\}_{k\in\mathcal{K}})$. We then set $\tilde{\boldsymbol{p}}_k^{\mathrm{prev}} = \tilde{\boldsymbol{p}}_k^{\mathrm{opt}}$ and $t^{\mathrm{prev}} = t^{\mathrm{opt}}$ and repeat these processes until $\{\tilde{\boldsymbol{p}}_k\}_{k\in\mathcal{K}}$ converges, thereby obtaining a near-optimal solution of $\mathscr{P}_3$.

After solving $\mathscr{P}_3$, we set $\tilde{\boldsymbol{p}}_k^{\mathrm{prev}} = \tilde{\boldsymbol{p}}_k$ and then update $\omega_{l,k}$ using (30). We repeat the alternating steps until the sparsity constraint (29c) is satisfied. Once we have $\{\tilde{\boldsymbol{p}}_k\}_{k\in\mathcal{K}}$, we can obtain the LEO satellite cluster indices and the power weights from $\{\tilde{\boldsymbol{p}}_k\}_{k\in\mathcal{K}}$ as $\mathcal{L}_k = \{l \in \mathcal{L} \mid \mathbb{1}_{\mathbb{R}^+}(\tilde{p}_{l,k}) = 1\}$ and $p_{l,k} = \tilde{p}_{l,k}$ for all $l \in \mathcal{L}_k$ and $k \in \mathcal{K}$, respectively. Algorithm 1 summarizes the proposed user-centric LEO satellite clustering and cooperative power allocation algorithm.

D. Computational Complexity Analysis

The proposed algorithm primarily consists of an outer iteration (i.e., re-weighted ℓ_2-norm approximation) and an inner iteration (i.e., SCA-based power allocation). In the inner iteration, the power allocation problem is formulated as an SOCP problem, which is then solved using the interior-point method. It has been shown that the computational complexity of the interior-point method for solving the SOCP problem with N_{var} variables is approximately $\mathcal{O}((N_{\mathrm{var}})^{3.5})$ [62]. Thus, the computational complexity of the SCA-based power allocation is $\mathcal{O}((LK)^{3.5}N_{\max}^{\mathrm{inner}})$ with $N_{\max}^{\mathrm{inner}}$ being the maximum number of SCA iterations. Thus, the overall computational complexity of the proposed algorithm is $\mathcal{O}((LK)^{3.5}N_{\max}^{\mathrm{inner}}N_{\max}^{\mathrm{outer}})$ where $N_{\max}^{\mathrm{outer}}$ is the maximum number of the outer iterations.

V. Achievable Rate Analysis: CF-mNTN Versus Conventional CF-MIMO System

A major distinctive feature of the proposed CF-mNTN over the conventional CF-mMIMO system is that the downlink data precoding of CF-mNTN is performed based on the statistical CSI, whereas that of CF-mMIMO system relies on the instantaneous CSI. While the instantaneous CSI-based precoding might be effective in terrestrial networks with stationary APs, its performance will degrade severely in NTN due to the channel estimation error caused by the high mobility of LEO satellites. To demonstrate this behavior, in this section, we derive the achievable rate of CF-mMIMO system and then compare it with that of CF-mNTN.

A. Achievable Rate Analysis of Conventional CF-mMIMO

In the conventional CF-mMIMO system, based on the channel reciprocity of time-division duplexing (TDD) systems, the LEO satellites acquire the instantaneous downlink CSI from the uplink pilot signals of UEs. Specifically, let $\boldsymbol{\psi}_k \in \mathbb{C}^{\tau_{\mathrm{p}}}$ be the pilot sequence intended for the kth UE such that $\|\boldsymbol{\psi}_k\|_2 = 1$, where τ_{p} is the pilot sequence length. Then the received pilot signal $\mathbf{Y}_l \in \mathbb{C}^{N\times\tau_{\mathrm{p}}}$ of the lth LEO satellite is

$$\mathbf{Y}_l = \sqrt{\eta_{\mathrm{t}}}\sum_{j=1}^{K}\mathbf{h}_{l,j}\boldsymbol{\psi}_j^{\mathrm{H}} + \mathbf{N}_l \tag{38}$$

where η_{t} is the uplink transmit power of UE and $\mathbf{N}_l \sim \mathcal{CN}(\mathbf{0}_{N\times\tau_{\mathrm{p}}}, \sigma_{\mathrm{n}}^2\boldsymbol{I}_N)$ is the complex Gaussian noise. To extract $\mathbf{h}_{l,k}$ from $\mathbf{Y}_l$, the lth LEO satellite projects $\mathbf{Y}_l$ onto $\boldsymbol{\psi}_k$ and then obtain the processed signal $\tilde{\mathbf{y}}_{l,k} \in \mathbb{C}^N$ as

$$\tilde{\mathbf{y}}_{l,k} \triangleq \frac{1}{\sqrt{\eta_{\mathrm{t}}}}\mathbf{Y}_l\boldsymbol{\psi}_k \tag{39}$$

$$= \mathbf{h}_{l,k} + \sum_{j\neq k}\mathbf{h}_{l,j}\boldsymbol{\psi}_j^{\mathrm{H}}\boldsymbol{\psi}_k + \frac{1}{\sqrt{\eta_{\mathrm{t}}}}\tilde{\mathbf{n}}_{l,k} \tag{40}$$

where $\tilde{\mathbf{n}}_{l,k} \triangleq \mathbf{N}_l\boldsymbol{\psi}_k \in \mathbb{C}^N$. Note that the second term of (40) is attributed to the non-orthogonality between the downlink pilot sequences (i.e., pilot contamination effect) [63].

Remark 1: The channel estimation accuracy of conventional CF-mMIMO system can be significantly deteriorated by the non-orthogonality between the uplink pilot sequences of UEs (i.e., $\tau_{\mathrm{p}} < K$) [63]. This so-called pilot contamination effect becomes more pronounced in NTN due to the short coherence time of LEO satellite channel. □

For a given $\tilde{\mathbf{y}}_{l,k}$, the minimum mean square error (MMSE) estimate $\hat{\mathbf{h}}_{l,k}$ of $\mathbf{h}_{l,k}$ is given by

$$\hat{\mathbf{h}}_{l,k} = \mathbb{E}\{\mathbf{h}_{l,k}\} + \mathbb{C}\mathrm{ov}\{\mathbf{h}_{l,k}, \tilde{\mathbf{y}}_{l,k}\}\,\mathbb{V}\{\tilde{\mathbf{y}}_{l,k}\}^{-1} \times (\tilde{\mathbf{y}}_{l,k} - \mathbb{E}\{\tilde{\mathbf{y}}_{l,k}\}) \tag{41}$$

$$= e^{j\phi_{l,k}}\sqrt{\kappa_{l,k}v_{l,k}}\,\boldsymbol{a}_{l,k} + v_{l,k}\boldsymbol{a}_{l,k}^{\mathrm{H}}\boldsymbol{V}_{l,k}^{-1} \times \left(\tilde{\mathbf{y}}_{l,k} - \sum_{j=1}^{K}\boldsymbol{\psi}_j^{\mathrm{H}}\boldsymbol{\psi}_k e^{j\phi_{l,j}}\sqrt{\kappa_{l,j}v_{l,j}}\,\boldsymbol{a}_{l,j}\right)\boldsymbol{a}_{l,k} \tag{42}$$

where

$$\boldsymbol{V}_{l,k} \triangleq \mathbb{V}\{\tilde{\mathbf{y}}_{l,k}\} \tag{43}$$

$$= \sum_{j=1}^{K} v_{l,j} |\boldsymbol{\psi}_j^{\mathrm{H}} \boldsymbol{\psi}_k|^2 \boldsymbol{a}_{l,j} \boldsymbol{a}_{l,j}^{\mathrm{H}} + \frac{\sigma_{\mathrm{n}}^2}{\eta_{\mathrm{t}}} \boldsymbol{I}_N \,. \tag{44}$$

Also, the instantaneous MRT (iMRT) precoding vector $\mathbf{w}_{l,k}^{\mathrm{iMRT}} \in \mathbb{C}^N$ constructed from $\hat{\mathbf{h}}_{l,k}$ is defined as

$$\mathbf{w}_{l,k}^{\mathrm{iMRT}} \triangleq \frac{\hat{\mathbf{h}}_{l,k}}{\sqrt{\mathbb{E}\{\|\hat{\mathbf{h}}_{l,k}\|_2^2\}}} \tag{45}$$

$$= \frac{\hat{\mathbf{h}}_{l,k}}{\sqrt{N(\kappa_{l,k} + x_{l,k,k})\, v_{l,k}}} \tag{46}$$

where $x_{l,k,k} \triangleq v_{l,k} \boldsymbol{a}_{l,k}^{\mathrm{H}} \boldsymbol{V}_{l,k}^{-1} \boldsymbol{a}_{l,k}$ and (46) is from the property of MMSE estimate that $\mathbb{E}\{\hat{\mathbf{h}}_{l,k}\} = \mathbb{E}\{\mathbf{h}_{l,k}\}$ and $\mathbb{V}\{\hat{\mathbf{h}}_{l,k}\} = \mathbb{C}\mathrm{ov}\{\mathbf{h}_{l,k}, \tilde{\mathbf{y}}_{l,k}\} \mathbb{V}\{\tilde{\mathbf{y}}_{l,k}\}^{-1} \mathbb{C}\mathrm{ov}\{\mathbf{h}_{l,k}, \tilde{\mathbf{y}}_{l,k}\}$. After the downlink data precoding, the LEO satellites jointly transmit the precoded data and then the UEs decode the data using the statistical CSI (see (13)-(21)). Then, the downlink ergodic achievable rate R_k^{CFmMIMO} of the kth UE of the conventional CF-mMIMO system is given by

$$R_k^{\mathrm{CFmMIMO}} = \log_2 \left(1 + \frac{|\gamma_k^{\mathrm{ds}}|^2}{\mathbb{E}\{|\gamma_k^{\mathrm{bu}}|^2\} + \sum_{j \neq k} \mathbb{E}\{|\gamma_k^{\mathrm{ui}}|^2\} + \sigma_{\mathrm{n}}^2} \right) \tag{47}$$

where

$$\gamma_k^{\mathrm{ds}} \triangleq \mathbb{E}\left\{ \sqrt{\rho_{\mathrm{t}}} \sum_{l \in \mathcal{L}_k} p_{l,k} \mathbf{h}_{l,k}^{\mathrm{H}} \mathbf{w}_{l,k}^{\mathrm{iMRT}} \right\} \tag{48}$$

$$\gamma_k^{\mathrm{bu}} \triangleq \sqrt{\rho_{\mathrm{t}}} \sum_{l \in \mathcal{L}_k} p_{l,k} \mathbf{h}_{l,k}^{\mathrm{H}} \mathbf{w}_{l,k} - \mathbb{E}\left\{ \sqrt{\rho_{\mathrm{t}}} \sum_{l \in \mathcal{L}_k} p_{l,k} \mathbf{h}_{l,k}^{\mathrm{H}} \mathbf{w}_{l,k}^{\mathrm{iMRT}} \right\} \tag{49}$$

$$\gamma_{k,j}^{\mathrm{ui}} \triangleq \sqrt{\rho_{\mathrm{t}}} \sum_{l \in \mathcal{L}_j} p_{l,j} \mathbf{h}_{l,k}^{\mathrm{H}} \mathbf{w}_{l,j}^{\mathrm{iMRT}} \,. \tag{50}$$

The following theorem provides the closed-form expression of R_k^{CFmMIMO} when using the iMRT precoding.

Theorem 2: The downlink achievable rate R_K^{CFmMIMO} of the k-th UE of the conventional CF-mMIMO using the iMRT precoding is expressed in (51), as shown at the bottom of the next page, where $x_{l,j,k} \triangleq v_{l,k} \boldsymbol{\psi}_k^{\mathrm{H}} \boldsymbol{\psi}_j \boldsymbol{a}_{l,j}^{\mathrm{H}} \boldsymbol{V}_{l,j}^{-1} \boldsymbol{a}_{l,k}$ for all $l \in \mathcal{L}$ and $k, j \in \mathcal{K}$. □

Proof: See Appendix B. ⊠

Remark 2: By comparing R_k^{CFmNTN} in (22) and R_k^{CFmMIMO} in (51), one can see that the distinction between R_k^{CFmNTN} and R_k^{CFmMIMO} lies in the terms $\{x_{l,j,k}\}_{l \in \mathcal{L}, k,j \in \mathcal{K}}$, which represents the non-orthogonality between the uplink pilot sequences of UEs. To be specific, since CF-mNTN exploits only the statistical CSI for the downlink data precoding, R_k^{CFmNTN} exhibits lower desired signal and beamforming uncertainty compared to R_k^{CFmMIMO}. Nevertheless, the desired signal degradation of CF-mNTN is marginal compared to the beamforming uncertainty degradation due to the LOS-dominant property of LEO satellite channel (i.e., $\kappa_{l,k} \gg 1$). □

B. Achievable Rate Comparison Between CF-mNTN and Conventional CF-mMIMO System

We consider the scenario where the LEO satellites are equipped with a large number of antennas to simplify the analysis.[3] In this scenario, one can exploit the mutual orthogonality between the array steering vectors, that is $|\boldsymbol{a}_{l,k}^{\mathrm{H}} \boldsymbol{a}_{l,j}| = N \delta_{k,j}$.

Proposition 1: When the number of antennas is large, the downlink achievable rate R_k^{CFmNTN} of the proposed CF-mNTN using sMRT and sZF precodings in (22) and the downlink achievable rate R_k^{CFmMIMO} of the conventional CF-mMIMO system using iMRT precoding in (51) are expressed as

$$R_k^{\mathrm{CFmNTN}} = \log_2 \left(1 + \frac{\rho_{\mathrm{t}} N \left(\sum_{l \in \mathcal{L}_k} p_{l,k} \sqrt{\kappa_{l,k} v_{l,k}} \right)^2}{\rho_{\mathrm{t}} N \sum_{l \in \mathcal{L}_k} p_{l,k}^2 v_{l,k} + \sigma_{\mathrm{n}}^2} \right) \tag{52}$$

$$R_k^{\mathrm{CFmMIMO}} = \log_2 \left(1 + \frac{\rho_{\mathrm{t}} N \left(\sum_{l \in \mathcal{L}_k} p_{l,k} \sqrt{(\kappa_{l,k} + x_{l,k,k}) v_{l,k}} \right)^2}{\rho_{\mathrm{t}} N \sum_{l \in \mathcal{L}_k} p_{l,k}^2 \left(1 + \frac{\kappa_{l,k} x_{l,k,k}}{\kappa_{l,k} + x_{l,k,k}} \right) v_{l,k} + \sigma_{\mathrm{n}}^2} \right) \tag{53}$$

where $x_{l,k,k} = \frac{\eta_{\mathrm{t}} N v_{l,k}}{\eta_{\mathrm{t}} N v_{l,k} + \sigma_{\mathrm{n}}^2}$ for all $l \in \mathcal{K}$ and $k \in \mathcal{K}$. □

Proof: See Appendix C. ⊠

For brevity, in the following lemma, we rewrite the achievable rate expressions in (52) and (53).

Lemma 1: Let $\boldsymbol{q}_k \triangleq \frac{1}{2} \left[p_{l,k} \sqrt{\frac{v_{l,k}}{\kappa_{l,k}}} \mid l \in \mathcal{L}_k \right]^{\mathrm{T}} \in \mathbb{R}^{|\mathcal{L}_k|}$, $r_k \triangleq \sum_{l \in \mathcal{L}_k} p_{l,k} \sqrt{\kappa_{l,k} v_{l,k}} \in \mathbb{R}$, $\boldsymbol{t}_k \triangleq \left[p_{l,k}^2 \frac{\kappa_{l,k} v_{l,k}}{\kappa_{l,k}+1} \mid l \in \mathcal{L}_k \right]^{\mathrm{T}} \in \mathbb{R}^{|\mathcal{L}_k|}$, $u_k \triangleq \sum_{l \in \mathcal{L}_k} p_{l,k}^2 v_{l,k} + \frac{\sigma_{\mathrm{n}}^2}{\rho_{\mathrm{t}} N} \in \mathbb{R}$, and $\boldsymbol{x}_k \triangleq [x_{l,k,k} \mid l \in \mathcal{L}_k]^{\mathrm{T}} \in \mathbb{R}^{|\mathcal{L}_k|}$. Also, let $h : \mathbb{R}^{|\mathcal{L}_k|} \to \mathbb{R}$ be the SINR function defined as $h(\boldsymbol{x}) \triangleq \frac{(\boldsymbol{q}_k^{\mathrm{T}} \boldsymbol{x} + r_k)^2}{\boldsymbol{t}_k^{\mathrm{T}} \boldsymbol{x} + u_k}$ for all $\boldsymbol{x} \in \mathbb{R}^{|\mathcal{L}_k|}$. Then R_k^{CFmNTN} and the upper bound of R_k^{CFmMIMO} can be simply expressed as

$$R_k^{\mathrm{CFmNTN}} = \log_2 \left(1 + h(\mathbf{0}_{|\mathcal{L}_k|}) \right) \tag{54}$$

$$R_k^{\mathrm{CFmMIMO}} \leqslant \log_2 \left(1 + h(\boldsymbol{x}_k) \right) . \tag{55}$$

□

Proof: The nominator of the upper bound of R_k^{CFmMIMO} in (55) can be obtained by using the inequality $\sqrt{1+x} \leqslant 1 + \frac{x}{2}$. Also, the denominator of the upper bound can be obtained from the facts that $x_{l,k,k} \in [0,1]$ and $\frac{\kappa_{l,k}}{\kappa_{l,k} + x_{l,k,k}} \geqslant \frac{\kappa_{l,k}}{\kappa_{l,k}+1}$. ⊠

Note that $h(\boldsymbol{x})$ is a convex function of $\boldsymbol{x}$. From the property of convex function, we get

$$h(\mathbf{0}_{|\mathcal{L}_k|}) \geqslant h(\boldsymbol{x}_k) - \nabla h(\boldsymbol{x}_k)^{\mathrm{T}} \boldsymbol{x}_k \,. \tag{56}$$

Now, we need to show that $\nabla h(\boldsymbol{x}_k)^{\mathrm{T}} \boldsymbol{x}_k \leqslant 0$. From the definition of $h(\boldsymbol{x}_k)$, one can see that this condition is equivalent to the following inequality:

$$\nabla h(\boldsymbol{x}_k)^{\mathrm{T}} \boldsymbol{x}_k \leqslant 0 \iff \frac{\boldsymbol{q}_k^{\mathrm{T}} \boldsymbol{x}_k}{r_k} \leqslant \frac{\boldsymbol{t}_k^{\mathrm{T}} \boldsymbol{x}_k}{\boldsymbol{t}_k^{\mathrm{T}} \boldsymbol{x}_k + 2u_k} \,. \tag{57}$$

The following proposition provides the sufficient condition for the inequality in (57) to hold.

[3] To achieve high throughput, high-frequency bands such as Ka-band (18 – 26.5 GHz), along with the massive satellite antenna array, are anticipated to be utilized in LEO satellite communication systems.

Proposition 2: Let $\kappa_{\min} \triangleq \min_{l\in\mathcal{L}_k,k\in\mathcal{K}} \kappa_{l,k}$ *and* $\alpha_{\min} \triangleq \min_{l\in\mathcal{L}_k,k\in\mathcal{K}} \frac{\eta_t N v_{l,k}}{\sigma_n^2}$. *In the high signal-to-noise ratio (SNR) regime, if* $(\kappa_{\min}-3)\,\alpha_{\min} \geqslant 1$ *is satisfied, then*

$$\frac{\boldsymbol{q}_k^{\mathrm{T}}\boldsymbol{x}_k}{r_k} \leqslant \frac{\boldsymbol{t}_k^{\mathrm{T}}\boldsymbol{x}_k}{\boldsymbol{t}_k^{\mathrm{T}}\boldsymbol{x}_k + 2u_k}. \tag{58}$$

□

Proof: See Appendix D. ⊠

In general, the sufficient condition $(\kappa_{\min}-3)\,\alpha_{\min} \geqslant 1$ in Proposition 2 holds due to the relatively low altitude of the LEO satellite and the LOS-dominant property of the LEO satellite channel. For example, in the 12 GHz Ku-band, the range of Rician K-factor is $10-20$ dB and the path loss of the terrestrial UE with a distance of 600 km from the 8×8-antenna LEO satellite is around $\beta \approx 2\times10^{-17}$ [64]. Considering that $v = \frac{\beta}{\kappa+1}$ and the UE uplink transmit power and noise power being $\eta_t = 30$ dBm and $\sigma_n^2 = -130$ dBm, respectively, we get $(\kappa-3)\,\alpha \geqslant 1.28$.

Finally, using Proposition 2, we obtain the desired result.

Theorem 3: In high SNR regime, if $(\kappa_{\min}-3)\,\alpha_{\min} \geqslant 1$ *is satisfied, then the downlink achievable rate* R_k^{CFmNTN} *of the proposed CF-mNTN surpasses the downlink achievable rate* R_k^{CFmMIMO} *of the conventional CF-mMIMO system.* □

Proof: This follows directly from Propositions 1 and 2, and Lemma 1. ⊠

VI. Numerical Results

A. Simulation Setup

In our simulations, we consider a LEO satellite mega-constellation systems where $L = 20$ LEO satellites cooperatively serve $K = 10$ UEs using the same time-frequency resources.[4] The maximum number of UEs (or UE groups) that each LEO satellite can simultaneously serve is $K_{\max} = 8$ [65]. We consider an $N = 8\times8$-element UPA antenna array at the LEO satellites and a single antenna at the UEs.[5] The orbital height and inclination of the LEO satellites are 550 km and 53°, respectively. The 3D coordinate vectors $\{\boldsymbol{p}_l^{\mathrm{sat}}\}_{l\in\mathcal{L}}$ of the LEO satellites are configured using the systems tool kit (STK), a space information network simulator, within a range of $700\times700\,\mathrm{km}^2$ [66]. Also, the coordinate vectors $\{\boldsymbol{p}_k^{\mathrm{ue}}\}_{k\in\mathcal{K}}$ of the UEs are randomly set within a circular service area of a radius 200 km. As for the channel model, we use the Rician fading model with carrier frequency $f = 5$ GHz and system bandwidth $B = 20$ MHz. The Rician K-factor $\{\kappa_{l,k}\}_{l\in\mathcal{L},k\in\mathcal{K}}$ are chosen randomly from 15-20 dB [64]. The antenna gains of LEO satellites and UEs are $G^{\mathrm{sat}} = 3$ dB and $G^{\mathrm{ue}} = 0$ dB. We set the downlink transmit power of LEO satellites, the uplink transmit power of UEs, and the noise power to $\rho_t = 40$ dBm, $\eta_t = 30$ dBm, and $\sigma_n^2 = -140$ dBm, respectively [23]. The regularization factor of the reweighted ℓ_2-norm approximation is $\epsilon = 10^{-10}$. As performance metrics, we use the sum-rate $R_{\mathrm{tot}} \triangleq \sum_{k=1}^{K} R_k$ and the minimum data rate $R_{\min} \triangleq \min_{k\in\mathcal{K}} R_k$. The simulations are conducted on MATLAB R2023B platform.

For comparison, we use 4 benchmark schemes: 1) a CF-mMIMO system where all LEO satellites jointly serve the UEs using the iMRT precoding [29]; 2) a single satellite system where the LEO satellite providing the highest received signal power serves the UE using the statistical signal-to-leakage-plus-noise ratio (SLNR)-based precoding [45]; 3) a single satellite system using the sMRT precoding; and 4) a spot beam-based system using 64 regional spot beams. To make a fair comparison, we employ the same SCA-based power allocation technique across all benchmark schemes. Note that in the conventional CF-mMIMO system, we use $\tau_p = 4$ pilot sequence for the uplink channel estimation.

B. Simulation Results

Fig. 3 shows the sum-rate as a function of SNR. We observe that the proposed CF-mNTN outperforms the conventional CF-mMIMO system by a large margin. For example, when SNR $= 30$ dB, CF-mNTN using sMRT precoding achieves more than 7.5% sum-rate improvement over the conventional CF-mMIMO system using iMRT precoding. Note that the performance of conventional CF-mMIMO system relies heavily on channel estimation accuracy, as the downlink precoding vectors are generated from the estimated instantaneous CSI. Thus, in NTN where the channel estimation error caused by the fast-varying characteristics of LEO satellite channel is unavoidable, the CF-mMIMO system suffers from substantial degradation of the data rate. In contrast, the performance of CF-mNTN is not affected by the channel estimation accuracy since the downlink precoding operation of CF-mNTN exploits only the statistical CSI acquired from the satellites and UEs positions. It is worth mentioning that in the low SNR regime, the sMRT precoding performs better than the sZF precoding, while in the high SNR regime, the sZF precoding outperforms the sMRT precoding.

Fig. 4 shows the sum-rate of CF-mNTN as a function of the number of LEO satellites L. We observe that the proposed CF-mNTN achieves significant sum-rate gains over the conventional single satellite systems as well as the spot

[4]The number of LEO satellites is determined based on the observation that the number of visible LEO satellites is typically around 20 to 30. Also, the number of UEs (or UE groups sharing the same statistical CSI) is determined based on the facts that the off-nadir angular resolution of an $N = 8\times8$-element planar antenna array is $\frac{2}{\sqrt{N}} \approx 14.3°$ and the maximum off-nadir angle of LEO satellite is around 40° ($\frac{40^2}{14.3^2} \approx 8$).

[5]Massive antenna arrays are expected to be deployed on LEO satellites to support high-frequency bands such as Ka-band (26.5-40 GHz).

$$R_k^{\mathrm{CFmMIMO}} = \log_2\left(1+\frac{\rho_t N\left(\sum_{l\in\mathcal{L}_k} p_{l,k}\sqrt{(\kappa_{l,k}+x_{l,k,k})\,v_{l,k}}\right)^2}{\frac{\rho_t}{N}\sum_{j=1}^{K}\sum_{l\in\mathcal{L}_j} p_{l,j}^2 v_{l,k}\left(1+\frac{\kappa_{l,k}x_{l,j,j}}{\kappa_{l,j}+x_{l,j,j}}\right)|\boldsymbol{a}_{l,k}^{\mathrm{H}}\boldsymbol{a}_{l,j}|^2 + \frac{\rho_t}{N}\sum_{j\neq k}\left|\sum_{l\in\mathcal{L}_j} p_{l,j}\frac{e^{j(\phi_{l,j}-\phi_{l,k})}\sqrt{\kappa_{l,k}\kappa_{l,j}v_{l,k}}+\sqrt{v_{l,j}}x_{l,j,k}}{\sqrt{\kappa_{l,j}+x_{l,j,j}}}\boldsymbol{a}_{l,k}^{\mathrm{H}}\boldsymbol{a}_{l,j}\right|^2 + \sigma_n^2}\right) \tag{51}$$

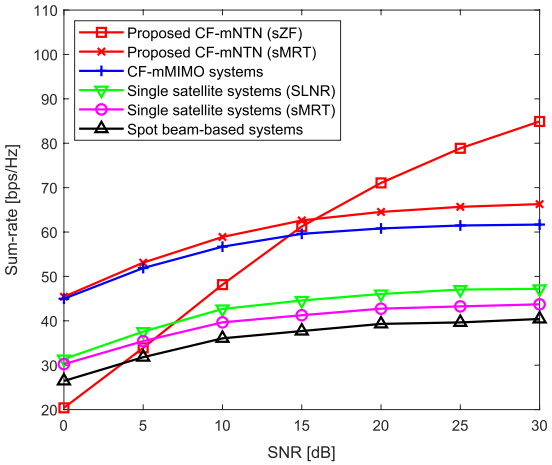

Fig. 3. Sum-rate as a function of SNR.

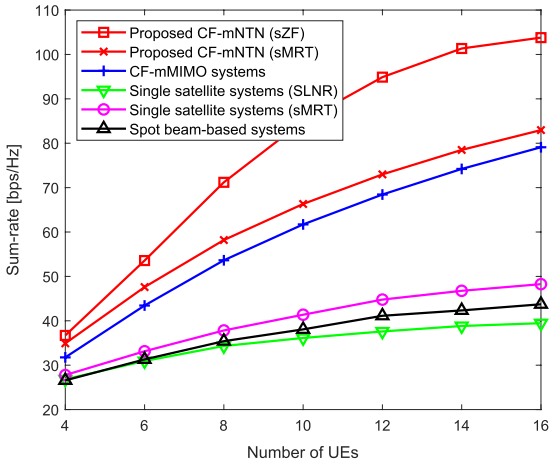

Fig. 5. Minimum data rate as a function of the number of LEO satellites.

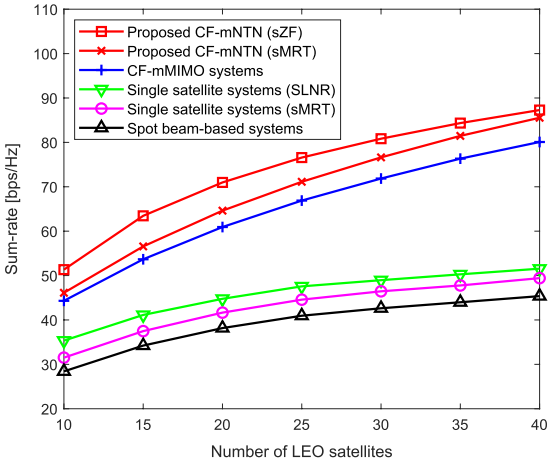

Fig. 4. Sum-rate as a function of the number of LEO satellites.

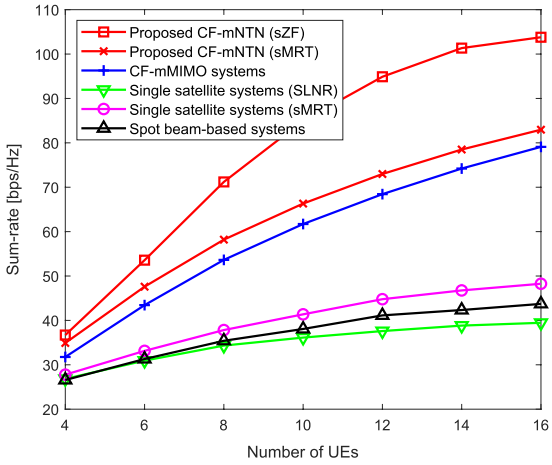

Fig. 6. Sum-rate as a function of the number of UEs.

beam-based system. Furthermore, we see that the sum-rate gains of CF-mNTN over the conventional single satellite systems increase with the number of LEO satellites. For example, when $L = 10$, the sum-rate gain of CF-mNTN using sZF precoding over the single satellite system using SLNR precoding is 45.2% but it increases up to 70% when $L = 40$. This is because CF-mNTN can effectively suppress the inter-satellite interferences through the user-centric satellite clustering and cooperative power allocation, whereas the conventional single satellite systems have no such mechanism to control the inter-satellite interferences.

To demonstrate the effectiveness of the proposed user-centric satellite clustering and cooperative power allocation algorithm, Fig. 5 compares the minimum data rate performance of the proposed algorithm with two benchmark schemes: 1) distance-based satellite clustering scheme that associates UE with the nearest LEO satellites; and 2) uniform power allocation scheme that distributes the transmit power equally among UEs. In this figure, we use the sMRT precoding for all schemes under test. We observe that the proposed algorithm outperforms the benchmark schemes. Even when compared to the scheme that uses the combination of distance-based satellite clustering and SCA-based power allocation, the proposed scheme improves the minimum data rate by 20%.

Fig. 6 shows the sum-rate as a function of the number of UEs K when SNR $= 30\,$dB. In this figure, we set $K_{\max} = \lfloor \frac{8K}{10} \rfloor$ so that $K_{\max}$ increases linearly with K. Interestingly, while the performance of CF-mNTN using sMRT precoding improves significantly with the number of UEs, that of CF-mNTN using sZF precoding converges gradually. The reason is that when the number of UEs is large, the geometric channel characteristics of distinct UEs become similar, leading to an increase in the correlation between the channel vectors of UEs. Note that the performance degradation of ZF precoding is much more severe in CF-mMIMO. This is because the large number of UEs increases not only the channel correlation but also the pilot contamination effect, resulting in a severe degradation of channel estimation accuracy. However, this is not the case for CF-mNTN as the estimation of instantaneous CSI is unnecessary for CF-mNTN.

Fig. 7 shows the sum-rate as a function of κ when $\kappa_{l,k} = \kappa$ for all $l \in \mathcal{L}, k \in \mathcal{K}$. We observe that when the Rician K-factor increases, the performance of the proposed CF-mNTN scheme increases gradually, whereas those of the single satellite systems remains unaffected. Recall that in CF-mNTN, the UE decodes the downlink data using the statistical CSI. Thus, when the Rician K-factor is high, the LEO satellite channel is dominated by the deterministic LOS component, leading

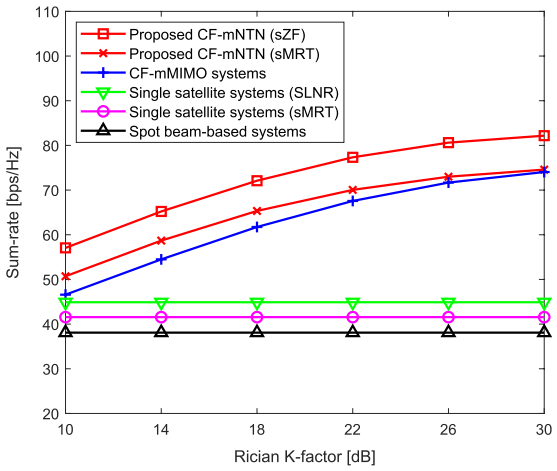

Fig. 7. Sum-rate as a function of Rician K-factor.

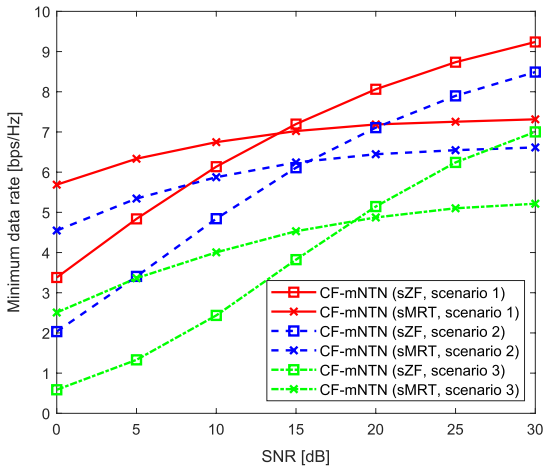

Fig. 9. Minimum data rate as a function of SNR.

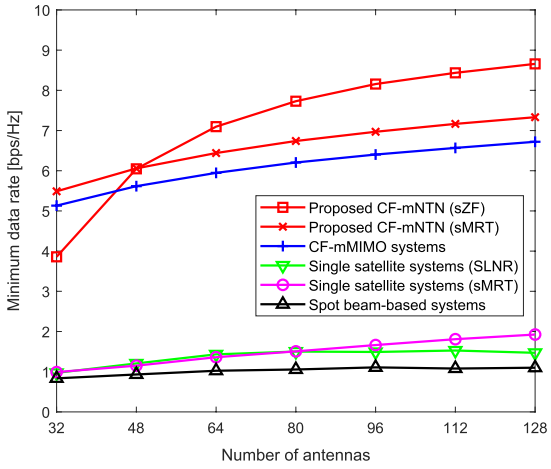

Fig. 8. Minimum data rate as a function of the number of antennas.

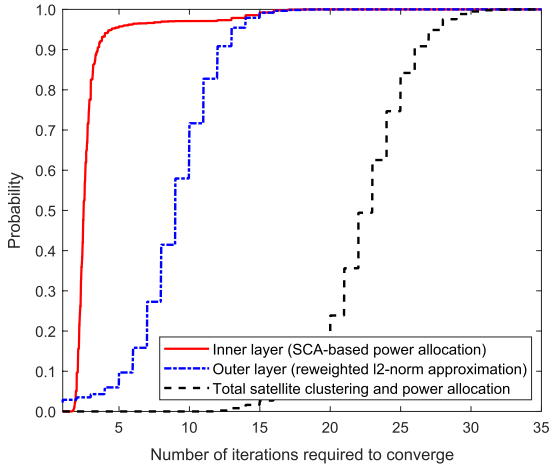

Fig. 10. Cumulative distribution of the number of iterations required to converge.

to reduced beamforming uncertainty (see (19)). Furthermore, when the Rician K-factor is high (e.g., $\kappa = 30\,\text{dB}$), the performance of CF-mNTN and that of conventional CF-mMIMO becomes similar as the random NLOS component of the LEO satellite channel becomes negligible.

Fig. 8 shows the minimum data rate as a function of the number of antennas N. We see that the proposed CF-mNTN significantly improves the minimum data rate over the conventional schemes. For example, when $N = 64$, CF-mNTN using sMRT precoding achieves 8.3%, 350%, 373%, and 529% minimum data rate improvements over the CF-mMIMO system using iMRT precoding, the single satellite systems using SLNR precoding and sMRT precoding, and the spot beam-based system, respectively. We also observe that the data rate gains of CF-mNTN increase with the number of antennas. In general, as the number of antennas increases, the correlations between the channel vectors of different UEs decrease. Considering that the key factor hindering the performance of CF-mNTN is IUI, it is clear that CF-mNTN would be more effective in massive MIMO regime.

To observe the performance variation of CF-mNTN under different system parameters, Fig. 9 shows the minimum data rate of CF-mNTN under three different scenarios: 1) a dense environment with $(L, K, N) = (30, 14, 96)$; 2) a moderate environment with $(L, K, N) = (20, 10, 64)$; and 3) a sparse environment with $(L, K, N) = (10, 6, 32)$. The performance of CF-mNTN is maximized in dense environments where the numbers of satellites, UEs, and antennas are large. This demonstrates that CF-mNTN is an effective means to ensure seamless connectivity in LEO satellite mega-constellation systems.

Fig. 10 shows the cumulative distributions of the number of iterations needed for the convergence of the inner layer iteration (SCA-based power allocation), outer layer iteration (reweighted ℓ_2-norm approximation), and total satellite clustering and power allocation algorithm. We observe that both SCA-based power allocation and reweighted ℓ_2-norm approximation converge within 20 iterations. We also observe that the proposed algorithm converges within 35 iterations.

VII. Conclusion

In this paper, we proposed a user-centric cooperative communication framework called CF-mNTN for xG LEO satellite mega-constellation systems. In contrast to the conventional

beam-centric systems where each UE is served by a single regional spot beam, in CF-mNTN, each UE is served by a cooperative group of LEO satellites. Since the LEO satellite clusters are dynamically organized based on the UE's communication environments, the handover frequency is substantially reduced. Moreover, since the inter-satellite interference is mitigated through the user-centric satellite clustering and cooperative power control, both the spectral efficiency and coverage are enhanced significantly. An intriguing feature of CF-mNTN is that we exploit only the statistical CSI for the satellite cooperation, data transmission, and reception. We demonstrated from the achievable rate analysis that the proposed CF-mNTN achieves higher achievable rates compared to the conventional CF-mMIMO system relying on the instantaneous CSI owing to the LOS-dominant and fast-varying characteristics of the LEO satellite channel. Also, from the numerical evaluations on realistic xG LEO satellite communication environments, we showed that CF-mNTN is very effective in improving the spectral efficiency and coverage.

APPENDIX A
PROOF OF THEOREM 1

For brevity, we denote the complex gain $\mathsf{g}_{l,k} \in \mathbb{C}$ of the LEO satellite channel $\mathbf{h}_{l,k}$ as

$$\mathsf{g}_{l,k} \triangleq \sqrt{\kappa_{l,k} v_{l,k}}\, e^{j\phi_{l,k}} + \sqrt{v_{l,k}}\, \boldsymbol{\alpha}_{l,k}\,. \tag{59}$$

Then, $\mathsf{g}_{l,k} \sim \mathcal{CN}(m_{l,k}, v_{l,k})$ where

$$m_{l,k} \triangleq \sqrt{\kappa_{l,k} v_{l,k}}\, e^{j\phi_{l,k}}\,. \tag{60}$$

Using $\mathsf{g}_{l,k}$, $\mathbf{h}_{l,k}$ in (8) can be rewritten as $\mathbf{h}_{l,k} = \mathsf{g}_{l,k}\boldsymbol{a}_{l,k}$. Also, we denote $\gamma_{k,j}$ as the effective channel gain as

$$\gamma_{k,j} \triangleq \sum_{l \in \mathcal{L}_j} p_{l,j} \mathbf{h}_{l,k}^{\mathrm{H}} \boldsymbol{w}_{l,j} = \sum_{l \in \mathcal{L}_j} p_{l,j} \mathsf{g}_{l,k}^{*} \boldsymbol{a}_{l,k}^{\mathrm{H}} \boldsymbol{w}_{l,j}\,. \tag{61}$$

Using $\gamma_{k,j}$, we can rewrite the desired signal, the beamforming uncertainty, and the IUI terms in (18)-(20) as

$$\gamma_k^{\mathrm{ds}} = \sqrt{\rho_{\mathrm{t}}}\, \mathbb{E}\{\gamma_{k,k}\} \tag{62}$$

$$\gamma_k^{\mathrm{bu}} = \sqrt{\rho_{\mathrm{t}}}\gamma_{k,k} - \sqrt{\rho_{\mathrm{t}}}\, \mathbb{E}\{\gamma_{k,k}\} \tag{63}$$

$$\gamma_{k,j}^{\mathrm{ui}} = \sqrt{\rho_{\mathrm{t}}}\gamma_{k,j}\,. \tag{64}$$

Next, we prove the statement in Theorem 1.

Proof: In CF-mNTN, $\boldsymbol{w}_{l,k}$ is a deterministic vector so the mean and variance of $\gamma_{k,j}$ are computed as

$$\mathbb{E}\{\gamma_{k,j}\} = \sum_{l \in \mathcal{L}_j} p_{l,j} m_{l,k} \boldsymbol{a}_{l,k}^{\mathrm{H}} \boldsymbol{w}_{l,j} \tag{65}$$

$$\mathbb{V}\{\gamma_{k,j}\} = \sum_{l \in \mathcal{L}_j} p_{l,j}^2 v_{l,k} \left|\boldsymbol{a}_{l,k}^{\mathrm{H}} \boldsymbol{w}_{l,j}\right|^2. \tag{66}$$

By substituting $\boldsymbol{w}_{l,k}$ with $\boldsymbol{w}_{l,k}^{\mathrm{sMRT}}$ and $\boldsymbol{w}_{l,k}^{\mathrm{sZF}}$ in (9) and (11), respectively, we obtain the desired results in (22). ☒

APPENDIX B
PROOF OF THEOREM 2

Proof: Using $\mathbf{h}_{l,k} = \mathsf{g}_{l,k}\boldsymbol{a}_{l,k}$ and the definition of $\mathbf{w}_{l,k}^{\mathrm{iMRT}}$ in (46), $\mathbb{E}\{\gamma_{k,j}\}$ of CF-mMIMO system is computed as

$$\mathbb{E}\{\gamma_{k,j}\} = \sum_{l \in \mathcal{L}_j} p_{l,j} \frac{\mathbb{E}\left\{\mathbf{h}_{l,k}^{\mathrm{H}} \hat{\mathbf{h}}_{l,j}\right\}}{\sqrt{\mathbb{E}\{\|\hat{\mathbf{h}}_{l,j}\|_2^2\}}} \tag{67}$$

$$= \sum_{l \in \mathcal{L}_j} \frac{p_{l,j} \boldsymbol{a}_{l,k}^{\mathrm{H}} \boldsymbol{a}_{l,j} \left(m_{l,j} \mathbb{E}\{\mathsf{g}_{l,k}^{*}\} + v_{l,j} \boldsymbol{a}_{l,j}^{\mathrm{H}} \boldsymbol{V}_{l,j}^{-1} \mathbb{E}\{\mathbf{c}\}\right)}{\sqrt{N(\kappa_{l,j} + x_{l,j,j}) v_{l,j}}} \tag{68}$$

$$= \sum_{l \in \mathcal{L}_j} p_{l,j} \frac{e^{j(\phi_{l,j} - \phi_{l,k})} \sqrt{\kappa_{l,k}\kappa_{l,j} v_{l,k}} + \sqrt{v_{l,j}} x_{l,j,k}}{\sqrt{N(\kappa_{l,j} + x_{l,j,j})}} \boldsymbol{a}_{l,k}^{\mathrm{H}} \boldsymbol{a}_{l,j} \tag{69}$$

where $\mathbf{c}$ is a random variable defined as

$$\mathbf{c} \triangleq \mathsf{g}_{l,k}^{*} \left(\tilde{\mathbf{y}}_{l,j} - \sum_{i=1}^{K} \boldsymbol{\psi}_i^{\mathrm{H}} \boldsymbol{\psi}_j m_{l,i} \boldsymbol{a}_{l,i}\right) \tag{70}$$

$$= \mathsf{g}_{l,k}^{*} \left(\sum_{i=1}^{K} \boldsymbol{\psi}_i^{\mathrm{H}} \boldsymbol{\psi}_j (\mathsf{g}_{l,i} - m_{l,i})\, \boldsymbol{a}_{l,i} + \frac{1}{\sqrt{\eta_{\mathrm{t}}}} \tilde{\mathbf{n}}_{l,k}\right). \tag{71}$$

Note that (71) is from the definition of $\tilde{\mathbf{y}}_{l,j}$ in (40). Also, $\mathbb{V}\{\gamma_{k,j}\}$ of CF-mMIMO system is computed as

$$\mathbb{V}\{\gamma_{k,j}\} = \sum_{l \in \mathcal{L}_j} p_{l,j}^2 \left|\boldsymbol{a}_{l,k}^{\mathrm{H}} \boldsymbol{a}_{l,j}\right|^2 \frac{\mathbb{V}\left\{m_{l,j} \mathsf{g}_{l,k}^{*} + v_{l,j} \boldsymbol{a}_{l,j}^{\mathrm{H}} \boldsymbol{V}_{l,j}^{-1} \mathbf{c}\right\}}{N(\kappa_{l,j} + x_{l,j,j})\, v_{l,j}} \tag{72}$$

$$= \sum_{l \in \mathcal{L}_j} \frac{p_{l,j}^2 |\boldsymbol{a}_{l,k}^{\mathrm{H}} \boldsymbol{a}_{l,j}|^2}{N(\kappa_{l,j} + x_{l,j,j})\, v_{l,j}} \Big(|m_{l,j}|^2 v_{l,k} + v_{l,j}^2 \boldsymbol{a}_{l,j}^{\mathrm{H}} \boldsymbol{V}_{l,j}^{-1} \mathbb{V}\{\mathbf{c}\}\, \boldsymbol{V}_{l,j}^{-1} \boldsymbol{a}_{l,j} + 2\Re\left\{m_{l,j} v_{l,j} \mathbb{C}\mathrm{ov}\left\{\mathsf{g}_{l,k}^{*}, \mathbf{c}\right\} \boldsymbol{V}_{l,j}^{-1} \boldsymbol{a}_{l,j}\right\}\Big) \tag{73}$$

where (73) is from the property that $\mathbb{V}\{\mathsf{x}+\mathsf{y}\} = \mathbb{V}\{\mathsf{x}\} + \mathbb{V}\{\mathsf{y}\} + 2\Re\{\mathbb{C}\mathrm{ov}\{\mathsf{x},\mathsf{y}\}\}$. From (71), $\mathbb{V}\{\mathbf{c}\}$ is computed as

$$\mathbb{V}\{\mathbf{c}\} = \sum_{i=1}^{K} \left|\boldsymbol{\psi}_i^{\mathrm{H}} \boldsymbol{\psi}_j\right|^2 \mathbb{V}\left\{\mathsf{g}_{l,k}^{*} (\mathsf{g}_{l,i} - m_{l,i})\right\} \boldsymbol{a}_{l,i} \boldsymbol{a}_{l,i}^{\mathrm{H}} + \mathbb{V}\left\{\mathsf{g}_{l,k}^{*} \tilde{\mathbf{n}}_{l,k}\right\} \tag{74}$$

$$= \left(|m_{l,k}|^2 + v_{l,k}\right) \left(\sum_{i=1}^{K} \left|\boldsymbol{\psi}_i^{\mathrm{H}} \boldsymbol{\psi}_j\right|^2 v_{l,i} \boldsymbol{a}_{l,i} \boldsymbol{a}_{l,i}^{\mathrm{H}} + \frac{\sigma_{\mathrm{n}}^2}{\eta_{\mathrm{t}}} \boldsymbol{I}_N\right) \tag{75}$$

$$= \left(|m_{l,k}|^2 + v_{l,k}\right) \boldsymbol{V}_{l,j} \tag{76}$$

where (75) is from the facts that $\mathbb{V}\left\{\mathsf{g}_{l,k}^{*}(\mathsf{g}_{l,i} - m_{l,i})\right\} = \left(|m_{l,k}|^2 + v_{l,k}\right) v_{l,i}$ for all $i \in \mathcal{K}$ and $\mathbb{V}\left\{\mathsf{g}_{l,k}^{*} \tilde{\mathbf{n}}_{l,k}\right\} = \left(|m_{l,k}|^2 + v_{l,k}\right) \frac{\sigma_{\mathrm{n}}^2}{\eta_{\mathrm{t}}} \boldsymbol{I}_N$. Also, (76) is from the definition of $\boldsymbol{V}_{l,j}$ in (44). Similarly, we can obtain

$$\mathbb{C}\mathrm{ov}\left\{\mathsf{g}_{l,k}^{*}, \mathbf{c}\right\} = \mathbf{0}_N^{\mathrm{T}}\,. \tag{77}$$

By plugging (76) and (77) into (73), we obtain

$$\mathbb{V}\{\gamma_{k,j}\} = \sum_{l\in\mathcal{L}_j} \frac{p_{l,j}^2 |\boldsymbol{a}_{l,k}^{\mathrm{H}}\boldsymbol{a}_{l,j}|^2}{N(\kappa_{l,j}+x_{l,j,j})v_{l,j}} \Big(\kappa_{l,j}v_{l,j}v_{l,k} + v_{l,j}^2(\kappa_{l,k}v_{l,k}+v_{l,k})\,\boldsymbol{a}_{l,j}^{\mathrm{H}}\boldsymbol{V}_{l,j}^{-1}\boldsymbol{a}_{l,j}\Big) \tag{78}$$

$$= \sum_{l\in\mathcal{L}_j} p_{l,j}^2 \frac{v_{l,k}}{N}\Big(1+\frac{\kappa_{l,k}x_{l,j,j}}{\kappa_{l,j}+x_{l,j,j}}\Big)\big|\boldsymbol{a}_{l,k}^{\mathrm{H}}\boldsymbol{a}_{l,j}\big|^2 \tag{79}$$

where (78) and (79) are from $|m_{l,k}|^2 = \kappa_{l,k}v_{l,k}$ and $x_{l,j,j} = v_{l,j}\boldsymbol{a}_{l,j}^{\mathrm{H}}\boldsymbol{V}_{l,j}^{-1}\boldsymbol{a}_{l,j}$. Finally, by plugging (69) and (79) to (62)-(64) and then into (47), we obtain the desired result. ☒

Appendix C
Proof of Proposition 1

Proof: When N is sufficiently large, the IUI term $\gamma_{k,j}^{\mathrm{ui}}$ becomes zero due to the mutual orthogonality $\big|\boldsymbol{a}_{l,k}^{\mathrm{H}}\boldsymbol{a}_{l,j}\big| = N\delta_{k,j}$ (see (61) and (64)). Also, we can rewrite $\boldsymbol{V}_{l,k}^{-1}$ as

$$\boldsymbol{V}_{l,k}^{-1} = \Big(\boldsymbol{A}_l\boldsymbol{\Sigma}_{l,k}\boldsymbol{A}_l^{\mathrm{H}} + \frac{\sigma_{\mathrm{n}}^2}{\eta_{\mathrm{t}}}\boldsymbol{I}_N\Big)^{-1} \tag{80}$$

$$= \frac{\eta_{\mathrm{t}}}{\sigma_{\mathrm{n}}^2}\Big(\boldsymbol{I}_N - \boldsymbol{A}_l\Big(\frac{\sigma_{\mathrm{n}}^2}{\eta_{\mathrm{t}}}\boldsymbol{\Sigma}_{l,k}^{-1} + N\boldsymbol{I}_N\Big)^{-1}\boldsymbol{A}_l^{\mathrm{H}}\Big) \tag{81}$$

where $\boldsymbol{A}_l \triangleq [\,\boldsymbol{a}_{l,1}\,\boldsymbol{a}_{l,2}\cdots\boldsymbol{a}_{l,K}\,]$ and $\boldsymbol{\Sigma}_{l,k} \triangleq \mathrm{diag}\big(|\boldsymbol{\psi}_1^{\mathrm{H}}\boldsymbol{\psi}_k|^2 v_{l,1}, |\boldsymbol{\psi}_2^{\mathrm{H}}\boldsymbol{\psi}_k|^2 v_{l,2}, \cdots, |\boldsymbol{\psi}_K^{\mathrm{H}}\boldsymbol{\psi}_k|^2 v_{l,K}\big)$. Then, $x_{l,j,k}$ can be rewritten as

$$x_{l,j,k} = v_{l,k}\boldsymbol{a}_{l,j}^{\mathrm{H}}\boldsymbol{V}_{l,j}^{-1}\boldsymbol{a}_{l,k} \tag{82}$$

$$= \frac{\eta_{\mathrm{t}}}{\sigma_{\mathrm{n}}^2}\boldsymbol{a}_{l,j}^{\mathrm{H}}\Big(\boldsymbol{I}_N - \boldsymbol{A}_l\Big(\frac{\sigma_{\mathrm{n}}^2}{\eta_{\mathrm{t}}}\boldsymbol{\Sigma}_{l,k}^{-1} + N\boldsymbol{I}_N\Big)^{-1}\boldsymbol{A}_l^{\mathrm{H}}\Big)\boldsymbol{a}_{l,k} \tag{83}$$

$$= \delta_{j,k}\frac{\eta_{\mathrm{t}}Nv_{l,k}}{\eta_{\mathrm{t}}Nv_{l,k}+\sigma_{\mathrm{n}}^2}\,. \tag{84}$$

By plugging (84) into (51), we obtain the desired results. ☒

Appendix D
Proof of Proposition 2

Proof: In the regime where SNR and N are high, $\rho_{\mathrm{t}}N \gg \sigma_{\mathrm{n}}^2$ holds true so one can effectively approximate u_k as

$$u_k = \sum_{l\in\mathcal{L}_k} p_{l,k}^2 v_{l,k} + \frac{\sigma_{\mathrm{n}}^2}{\rho_{\mathrm{t}}N} \approx \sum_{l\in\mathcal{L}_k} p_{l,k}^2 v_{l,k}\,. \tag{85}$$

Also, from the definition of $\alpha_{\min}$, we have $\eta_{\mathrm{t}}Nv_{l,k} \geqslant \alpha_{\min}\sigma_{\mathrm{n}}^2$ and $x_{l,k,k} = \frac{\eta_{\mathrm{t}}Nv_{l,k}}{\eta_{\mathrm{t}}Nv_{l,k}+\sigma_{\mathrm{n}}^2} \geqslant \frac{\alpha_{\min}}{\alpha_{\min}+1}$. Using these, we obtain

$$\frac{\boldsymbol{t}_k^{\mathrm{T}}\boldsymbol{x}_k}{\boldsymbol{t}_k^{\mathrm{T}}\boldsymbol{x}_k + 2u_k} \geqslant \frac{\frac{\alpha_{\min}}{\alpha_{\min}+1}\sum_{l\in\mathcal{L}_k} p_{l,k}^2 \frac{\kappa_{\min}v_{l,k}}{\kappa_{\min}+1}}{\frac{\alpha_{\min}}{\alpha_{\min}+1}\sum_{l\in\mathcal{L}_k} p_{l,k}^2 \frac{\kappa_{\min}v_{l,k}}{\kappa_{\min}+1} + 2\sum_{l\in\mathcal{L}_k} p_{l,k}^2 v_{l,k}} \tag{86}$$

$$= \frac{\frac{\kappa_{\min}\alpha_{\min}}{(\kappa_{\min}+1)(\alpha_{\min}+1)}}{\frac{\kappa_{\min}\alpha_{\min}}{(\kappa_{\min}+1)(\alpha_{\min}+1)}+2}\,. \tag{87}$$

By comparing $\boldsymbol{q}_k^{\mathrm{T}}\boldsymbol{x}_k$ and r_k, we obtain

$$\boldsymbol{q}_k^{\mathrm{T}}\boldsymbol{x}_k = \frac{1}{2}\sum_{l\in\mathcal{L}_k} p_{l,k}\sqrt{\frac{v_{l,k}}{\kappa_{l,k}}}\,x_{l,k} \tag{88}$$

$$\leqslant \frac{1}{2\kappa_{\min}}\sum_{l\in\mathcal{L}_k} p_{l,k}\sqrt{\kappa_{l,k}v_{l,k}} \tag{89}$$

$$= \frac{1}{2\kappa_{\min}}r_k\,. \tag{90}$$

Finally, by using (87), (90), and the condition $\kappa_{\min} \geqslant 3+\frac{1}{\alpha_{\min}}$, we obtain the desired result in (58) as

$$\frac{r_k(\boldsymbol{t}_k^{\mathrm{T}}\boldsymbol{x}_k)}{(\boldsymbol{q}_k^{\mathrm{T}}\boldsymbol{x}_k)(\boldsymbol{t}_k^{\mathrm{T}}\boldsymbol{x}_k+2u_k)} \geqslant \frac{\frac{2\kappa_{\min}^2\alpha_{\min}}{(\kappa_{\min}+1)(\alpha_{\min}+1)}}{\frac{\kappa_{\min}\alpha_{\min}}{(\kappa_{\min}+1)(\alpha_{\min}+1)}+2} \tag{91}$$

$$\geqslant \frac{\frac{2(3\alpha_{\min}+1)^2}{(4\alpha_{\min}+1)(\alpha_{\min}+1)}}{\frac{(3\alpha_{\min}+1)\alpha_{\min}}{(4\alpha_{\min}+1)(\alpha_{\min}+1)}+2} \tag{92}$$

$$= \frac{18\alpha_{\min}^2+12\alpha_{\min}+2}{11\alpha_{\min}^2+11\alpha_{\min}+2} \tag{93}$$

$$\geqslant 1\,. \tag{94}$$

☒

References

[1] S. Dang, O. Amin, B. Shihada, and M.-S. Alouini, "What should 6G be?" *Nature Electron.*, vol. 3, no. 1, pp. 20–29, Jan. 2020.

[2] A. Conti et al., "Location awareness in beyond 5G networks," *IEEE Commun. Mag.*, vol. 59, no. 11, pp. 22–27, Nov. 2021.

[3] Z. Zhang et al., "6G wireless networks: Vision, requirements, architecture, and key technologies," *IEEE Veh. Technol. Mag.*, vol. 14, no. 3, pp. 28–41, Sep. 2019.

[4] F. Morselli, S. M. Razavi, M. Z. Win, and A. Conti, "Soft information based localization for 5G networks and beyond," *IEEE Trans. Wireless Commun.*, vol. 22, no. 12, pp. 9923–9938, Dec. 2023.

[5] *Technical Specification Group Radio Access Network; Solutions for NR to Support Non-Terrestrial Networks (NTN) (Release 16)*, Standard 3GPP TR 38.821 V16.2.0, Release 16, 3rd Generation Partnership Project, Mar. 2023.

[6] *Technical Specification Group Radio Access Network; NR; User Equipment (UE) Feature List (Release 17)*, Standard 3GPP TR 38.822 V17.1.0, Release 17, 3rd Generation Partnership Project, Jun. 2023.

[7] *Technical Specification Group Radio Access Network; Non-Terrestrial Networks (NTN) L-/S-Band for NR (Release 18)*, Standard 3GPP TR 38.741 V18.1.0, Release 18, 3rd Generation Partnership Project, Mar. 2024.

[8] A. Alsharoa and M.-S. Alouini, "Improvement of the global connectivity using integrated satellite-airborne-terrestrial networks with resource optimization," *IEEE Trans. Wireless Commun.*, vol. 19, no. 8, pp. 5088–5100, Aug. 2020.

[9] M. M. Azari et al., "Evolution of non-terrestrial networks from 5G to 6G: A survey," *IEEE Commun. Surveys Tuts.*, vol. 24, no. 4, pp. 2633–2672, 4th Quart., 2022.

[10] F. Rinaldi et al., "Non-terrestrial networks in 5G & beyond: A survey," *IEEE Access*, vol. 8, pp. 165178–165200, 2020.

[11] G. Kwon, W. Shin, A. Conti, W. C. Lindsey, and M. Z. Win, "Access-backhaul strategy via gNB cooperation for integrated terrestrial-satellite networks," *IEEE J. Sel. Areas Commun.*, vol. 42, no. 5, pp. 1403–1419, May 2024.

[12] X. Lin, S. Cioni, G. Charbit, N. Chuberre, S. Hellsten, and J. Boutillon, "On the path to 6G: Embracing the next wave of low earth orbit satellite access," *IEEE Commun. Mag.*, vol. 59, no. 12, pp. 36–42, Dec. 2021.

[13] R. Deng, B. Di, H. Zhang, L. Kuang, and L. Song, "Ultra-dense LEO satellite constellations: How many LEO satellites do we need?" *IEEE Trans. Wireless Commun.*, vol. 20, no. 8, pp. 4843–4857, Aug. 2021.

[14] Z. Qu, G. Zhang, H. Cao, and J. Xie, "LEO satellite constellation for Internet of Things," *IEEE Access*, vol. 5, pp. 18391–18401, 2017.

[15] B. Al Homssi et al., "Next generation mega satellite networks for access equality: Opportunities, challenges, and performance," *IEEE Commun. Mag.*, vol. 60, no. 4, pp. 18–24, Apr. 2022.

[16] P. Chowdhury, M. Atiquzzaman, and W. Ivancic, "Handover schemes in satellite networks: State-of-the-art and future research directions," *IEEE Commun. Surveys Tuts.*, vol. 8, no. 4, pp. 2–14, 4th Quart., 2006.

[17] Y. Su, Y. Liu, Y. Zhou, J. Yuan, H. Cao, and J. Shi, "Broadband LEO satellite communications: Architectures and key technologies," *IEEE Wireless Commun.*, vol. 26, no. 2, pp. 55–61, Apr. 2019.

[18] J. Tang, D. Bian, G. Li, J. Hu, and J. Cheng, "Optimization method of dynamic beam position for LEO beam-hopping satellite communication systems," *IEEE Access*, vol. 9, pp. 57578–57588, 2021.

[19] A. Ivanov, R. Bychkov, and E. Tcatcorin, "Spatial resource management in LEO satellite," *IEEE Trans. Veh. Technol.*, vol. 69, no. 12, pp. 15623–15632, Dec. 2020.

[20] E. Kim, I. P. Roberts, and J. G. Andrews, "Downlink analysis and evaluation of multi-beam LEO satellite communication in shadowed Rician channels," *IEEE Trans. Veh. Technol.*, vol. 73, no. 2, pp. 2061–2075, Feb. 2024.

[21] L. Lei et al., "Spatial–temporal resource optimization for uneven-traffic LEO satellite systems: Beam pattern selection and user scheduling," *IEEE J. Sel. Areas Commun.*, vol. 42, no. 5, pp. 1279–1291, May 2024.

[22] Z. Lin, Z. Ni, L. Kuang, C. Jiang, and Z. Huang, "Dynamic beam pattern and bandwidth allocation based on multi-agent deep reinforcement learning for beam hopping satellite systems," *IEEE Trans. Veh. Technol.*, vol. 71, no. 4, pp. 3917–3930, Apr. 2022.

[23] K.-X. Li et al., "Downlink transmit design for massive MIMO LEO satellite communications," *IEEE Trans. Commun.*, vol. 70, no. 2, pp. 1014–1028, Feb. 2022.

[24] L. You et al., "Hybrid analog/digital precoding for downlink massive MIMO LEO satellite communications," *IEEE Trans. Wireless Commun.*, vol. 21, no. 8, pp. 5962–5976, Aug. 2022.

[25] Y. Liu, C. Li, J. Li, and L. Feng, "Robust energy-efficient hybrid beamforming design for massive MIMO LEO satellite communication systems," *IEEE Access*, vol. 10, pp. 63085–63099, 2022.

[26] M. Lin, Z. Lin, W.-P. Zhu, and J.-B. Wang, "Joint beamforming for secure communication in cognitive satellite terrestrial networks," *IEEE J. Sel. Areas Commun.*, vol. 36, no. 5, pp. 1017–1029, May 2018.

[27] Q. Wang, H. Zhang, J.-B. Wang, F. Yang, and G. Y. Li, "Joint beamforming for integrated mmWave satellite-terrestrial self-backhauled networks," *IEEE Trans. Veh. Technol.*, vol. 70, no. 9, pp. 9103–9117, Sep. 2021.

[28] D. Peng, A. Bandi, Y. Li, S. Chatzinotas, and B. Ottersten, "Hybrid beamforming, user scheduling, and resource allocation for integrated terrestrial-satellite communication," *IEEE Trans. Veh. Technol.*, vol. 70, no. 9, pp. 8868–8882, Sep. 2021.

[29] M. Y. Abdelsadek, G. K. Kurt, and H. Yanikomeroglu, "Distributed massive MIMO for LEO satellite networks," *IEEE Open J. Commun. Soc.*, vol. 3, pp. 2162–2177, 2022.

[30] X. Zhang, S. Sun, M. Tao, Q. Huang, and X. Tang, "Multi-satellite cooperative networks: Joint hybrid beamforming and user scheduling design," *IEEE Trans. Wireless Commun.*, vol. 23, no. 7, pp. 7938–7952, Jul. 2024.

[31] D. Kim, J. Park, and N. Lee, "Coverage analysis of dynamic coordinated beamforming for LEO satellite downlink networks," *IEEE Trans. Wireless Commun.*, vol. 23, no. 9, pp. 12239–12255, Sep. 2024.

[32] F. Wang, D. Jiang, Z. Wang, J. Chen, and T. Q. S. Quek, "Seamless handover in LEO based non-terrestrial networks: Service continuity and optimization," *IEEE Trans. Commun.*, vol. 71, no. 2, pp. 1008–1023, Feb. 2023.

[33] H. Zhou, J. Li, K. Yang, H. Zhou, J. An, and Z. Han, "Handover analysis in ultra-dense LEO satellite networks with beamforming methods," *IEEE Trans. Veh. Technol.*, vol. 72, no. 3, pp. 3676–3690, Mar. 2023.

[34] M. Jia, X. Zhang, X. Gu, Q. Guo, Y. Li, and P. Lin, "Interbeam interference constrained resource allocation for shared spectrum multibeam satellite communication systems," *IEEE Internet Things J.*, vol. 6, no. 4, pp. 6052–6059, Aug. 2019.

[35] M. Z. Win, Y. Shen, and W. Dai, "A theoretical foundation of network localization and navigation," *Proc. IEEE*, vol. 106, no. 7, pp. 1136–1165, Jul. 2018.

[36] R. Di Taranto, S. Muppirisetty, R. Raulefs, D. Slock, T. Svensson, and H. Wymeersch, "Location-aware communications for 5G networks: How location information can improve scalability, latency, and robustness of 5G," *IEEE Signal Process. Mag.*, vol. 31, no. 6, pp. 102–112, Nov. 2014.

[37] Z. Wang, Z. Liu, Y. Shen, A. Conti, and M. Z. Win, "Location awareness in beyond 5G networks via reconfigurable intelligent surfaces," *IEEE J. Sel. Areas Commun.*, vol. 40, no. 7, pp. 2011–2025, Jul. 2022.

[38] W. Stock, R. T. Schwarz, C. A. Hofmann, and A. Knopp, "Survey on opportunistic PNT with signals from LEO communication satellites," *IEEE Commun. Surveys Tuts.*, early access, May 30, 2024, doi: 10.1109/COMST.2024.3406990.

[39] M. Z. Win, Z. Wang, Z. Liu, Y. Shen, and A. Conti, "Location awareness via intelligent surfaces: A path toward holographic NLN," *IEEE Veh. Technol. Mag.*, vol. 17, no. 2, pp. 37–45, Jun. 2022.

[40] R. M. Ferre et al., "Is LEO-based positioning with mega-constellations the answer for future equal access localization?" *IEEE Commun. Mag.*, vol. 60, no. 6, pp. 40–46, Jun. 2022.

[41] A. Conti, G. Torsoli, C. A. Gómez-Vega, A. Vaccari, G. Mazzini, and M. Z. Win, "3GPP-compliant datasets for xG location-aware networks," *IEEE Open J. Veh. Technol.*, vol. 5, pp. 473–484, 2024.

[42] A. Conti, G. Torsoli, C. A. Gómez-Vega, A. Vaccari, and M. Z. Win, "xG-Loc: 3GPP-compliant datasets for xG location-aware networks," IEEE Dataport, Dec. 2023, doi: 10.21227/rper-vc03.

[43] H. Xv, Y. Sun, Y. Zhao, M. Peng, and S. Zhang, "Joint beam scheduling and beamforming design for cooperative positioning in multi-beam LEO satellite networks," *IEEE Trans. Veh. Technol.*, vol. 73, no. 4, pp. 5276–5287, Apr. 2024.

[44] A. Conti, S. Mazuelas, S. Bartoletti, W. C. Lindsey, and M. Z. Win, "Soft information for localization-of-things," *Proc. IEEE*, vol. 107, no. 11, pp. 2240–2264, Sep. 2019.

[45] L. You, K.-X. Li, J. Wang, X. Gao, X.-G. Xia, and B. Ottersten, "Massive MIMO transmission for LEO satellite communications," *IEEE J. Sel. Areas Commun.*, vol. 38, no. 8, pp. 1851–1865, Aug. 2020.

[46] V. Va, J. Choi, and R. W. Heath, "The impact of beamwidth on temporal channel variation in vehicular channels and its implications," *IEEE Trans. Veh. Technol.*, vol. 66, no. 6, pp. 5014–5029, Jun. 2016.

[47] H. Q. Ngo, A. Ashikhmin, H. Yang, E. G. Larsson, and T. L. Marzetta, "Cell-free massive MIMO versus small cells," *IEEE Trans. Wireless Commun.*, vol. 16, no. 3, pp. 1834–1850, Mar. 2017.

[48] E. Nayebi, A. Ashikhmin, T. L. Marzetta, H. Yang, and B. D. Rao, "Precoding and power optimization in cell-free massive MIMO systems," *IEEE Trans. Wireless Commun.*, vol. 16, no. 7, pp. 4445–4459, Jul. 2017.

[49] J. Zhang, S. Chen, Y. Lin, J. Zheng, B. Ai, and L. Hanzo, "Cell-free massive MIMO: A new next-generation paradigm," *IEEE Access*, vol. 7, pp. 99878–99888, 2019.

[50] S. Elhoushy, M. Ibrahim, and W. Hamouda, "Cell-free massive MIMO: A survey," *IEEE Commun. Surveys Tuts.*, vol. 24, no. 1, pp. 492–523, 1st Quart., 2022.

[51] M. Z. Win et al., "Network localization and navigation via cooperation," *IEEE Commun. Mag.*, vol. 49, no. 5, pp. 56–62, May 2011.

[52] T. Janssen, A. Koppert, R. Berkvens, and M. Weyn, "A survey on IoT positioning leveraging LPWAN, GNSS and LEO-PNT," *IEEE Internet Things J.*, vol. 10, no. 13, pp. 11135–11159, Feb. 2023.

[53] M. Z. Win, W. Dai, Y. Shen, G. Chrisikos, and H. V. Poor, "Network operation strategies for efficient localization and navigation," *Proc. IEEE*, vol. 106, no. 7, pp. 1224–1254, Jul. 2018.

[54] H. K. Dureppagari, C. Saha, H. S. Dhillon, and R. M. Buehrer, "NTN-based 6G localization: Vision, role of LEOs, and open problems," *IEEE Wireless Commun.*, vol. 30, no. 6, pp. 44–51, Dec. 2023.

[55] S. Kim, J. Moon, J. Wu, B. Shim, and M. Z. Win, "Vision-aided positioning and beam focusing for 6G terahertz communications," *IEEE J. Sel. Areas Commun.*, vol. 42, no. 9, pp. 2503–2519, Sep. 2024.

[56] Q. Zhang, S. Jin, M. McKay, D. Morales-Jimenez, and H. Zhu, "Power allocation schemes for multicell massive MIMO systems," *IEEE Trans. Wireless Commun.*, vol. 14, no. 11, pp. 5941–5955, Nov. 2015.

[57] J. W. Choi, B. Shim, Y. Ding, B. Rao, and D. I. Kim, "Compressed sensing for wireless communications: Useful tips and tricks," *IEEE Commun. Surveys Tuts.*, vol. 19, no. 3, pp. 1527–1550, 3rd Quart., 2017.

[58] S. Kim and B. Shim, "Energy-efficient millimeter-wave cell-free systems under limited feedback," *IEEE Trans. Commun.*, vol. 69, no. 6, pp. 4067–4082, Jun. 2021.

[59] E. J. Candes, M. B. Wakin, and S. P. Boyd, "Enhancing sparsity by reweighted ℓ_1 minimization," *J. Fourier Anal. Appl.*, vol. 14, nos. 5–6, pp. 877–905, Oct. 2008.

[60] A. Beck, A. Ben-Tal, and L. Tetruashvili, "A sequential parametric convex approximation method with applications to nonconvex truss topology design problems," *J. Global Optim.*, vol. 47, no. 1, pp. 29–51, May 2010.

[61] S. Boyd and L. Vandenberghe, *Convex Optimization*. Cambridge, U.K.: Cambridge Univ. Press, 2004.
[62] Y. Ye, *Interior Point Algorithms: Theory and Analysis*. Hoboken, NJ, USA: Wiley, 2011.
[63] J. Jose, A. Ashikhmin, T. L. Marzetta, and S. Vishwanath, "Pilot contamination and precoding in multi-cell TDD systems," *IEEE Trans. Wireless Commun.*, vol. 10, no. 8, pp. 2640–2651, Aug. 2011.
[64] *Technical Specification Group Radio Access Network; Study on New Radio (NR) to Support Non-Terrestrial Networks (Release 15)*, Standard 3GPPTR 38.811 V15.4.0, Release 15, 3rd Generation Partnership Project, Sep. 2020.
[65] J. Palacios, N. González-Prelcic, C. Mosquera, T. Shimizu, and C.-H. Wang, "A hybrid beamforming design for massive MIMO LEO satellite communications," *Frontiers Space Technol.*, vol. 2, pp. 1–14, Sep. 2021.
[66] W. Jiang, Y. Zhan, X. Xiao, and G. Sha, "Network simulators for satellite-terrestrial integrated networks: A survey," *IEEE Access*, vol. 11, pp. 98269–98292, 2023.

Seungnyun Kim (Member, IEEE) received the B.S. (with honor) and Ph.D. degrees in electrical and computer engineering from Seoul National University (SNU), Seoul, South Korea, in 2016 and 2023, respectively.

He is currently a Postdoctoral Fellow with the Wireless Information and Network Sciences Laboratory, Massachusetts Institute of Technology, Cambridge, MA, USA. His research interests include information theory, optimization methods, and machine learning with applications to real-world problems, including wireless communications, network localization and navigation, and non-terrestrial networks.

Dr. Kim was a recipient of the Sejong Science Fellowship from Korean Government in 2023, the Best Ph.D. Dissertation Award from SNU in 2023, the Qualcomm Innovation Fellowship Finalist in 2021, and the Samsung Humantech Paper Award Gold Prize in 2019.

Jiao Wu (Member, IEEE) received the B.S. degree in communication engineering from North China Electric Power University (NCEPU), Beijing, China, in 2015, the M.S. degree in electronics and communication engineering from the University of Electronic Science and Technology of China (UESTC), Chengdu, China, in 2018, and the Ph.D. degree in electrical and computer engineering from Seoul National University (SNU), Seoul, South Korea, in 2023.

She is currently a Postdoctoral Fellow with the Computer, Electrical and Mathematical Sciences and Engineering Division (CEMSE), King Abdullah University of Science and Technology (KAUST), Thuwal, Saudi Arabia. Her research interests include signal processing, optimization techniques, and machine learning with applications to reconfigurable intelligent surfaces-assisted communications, extremely large-scale antenna systems, integrated sensing and communications, and non-terrestrial networks.

Byonghyo Shim (Senior Member, IEEE) received the B.S. and M.S. degrees in control and instrumentation engineering from Seoul National University, South Korea, in 1995 and 1997, respectively, and the M.S. degree in mathematics and the Ph.D. degree in electrical and computer engineering from the University of Illinois at Urbana–Champaign (UIUC), Champaign, IL, USA, in 2004 and 2005, respectively.

From 1997 to 2000, he was an Officer (First Lieutenant) and an Academic Instructor (full-time) with the Department of Electronics Engineering, Korean Air Force Academy. From 2005 to 2007, he was a Staff Engineer with Qualcomm Inc., San Diego, CA, USA. From 2007 to 2014, he was an Associate Professor with the School of Information and Communication, Korea University, Seoul. Since 2014, he has been with Seoul National University (SNU), where he is currently a Professor with the Department of Electrical and Computer Engineering and the Director of the Institute of New Media and Communications. His research interests include wireless communications, statistical signal processing, and deep learning.

Dr. Shim was an elected Member of the Signal Processing for Communications and Networking (SPCOM) Technical Committee of the IEEE Signal Processing Society. He was a recipient of the M. E. Van Valkenburg Research Award from the ECE Department, University of Illinois, in 2005; the Hadong Young Engineer Award from IEIE in 2010; the Irwin Jacobs Award from Qualcomm and KICS in 2016; the Shinyang Research Award from the Engineering College of SNU in 2017; the Okawa Foundation Research Award in 2020; the IEEE Comsoc AP Outstanding Paper Award in 2021; and the JCN Best Paper Award in 2024. He has served as an Associate Editor for IEEE TRANSACTIONS ON WIRELESS COMMUNICATIONS, IEEE TRANSACTIONS ON COMMUNICATIONS, IEEE TRANSACTIONS ON VEHICULAR TECHNOLOGY, IEEE TRANSACTIONS ON SIGNAL PROCESSING, IEEE WIRELESS COMMUNICATIONS LETTERS, and *Journal of Communications and Networks*; and a Guest Editor for IEEE JOURNAL ON SELECTED AREAS IN COMMUNICATIONS.

Moe Z. Win (Fellow, IEEE) is the Robert R. Taylor Professor at the Massachusetts Institute of Technology (MIT) and the founding director of the Wireless Information and Network Sciences Laboratory. Prior to joining MIT, he was with AT&T Research Laboratories and with the NASA Jet Propulsion Laboratory.

His research encompasses fundamental theories, algorithm design, and network experimentation for a broad range of real-world problems. His current research topics include ultra-wideband systems, network localization and navigation, network interference exploitation, and quantum information science. He has served the IEEE Communications Society as an elected Member-at-Large on the Board of Governors, as elected Chair of the Radio Communications Committee, and as an IEEE Distinguished Lecturer. Over the last two decades, he held various editorial positions for IEEE journals and organized numerous international conferences. He has served on the SIAM Diversity Advisory Committee.

Dr. Win is an elected Fellow of the AAAS, the EURASIP, the IEEE, and the IET. He was honored with two IEEE Technical Field Awards: the IEEE Kiyo Tomiyasu Award (2011) and the IEEE Eric E. Sumner Award (2006, jointly with R. A. Scholtz). His publications, co-authored with students and colleagues, have received several awards. Other recognitions include the MIT Frank E. Perkins Award (2024), the MIT Everett Moore Baker Award (2022), the IEEE Vehicular Technology Society James Evans Avant Garde Award (2022), the IEEE Communications Society Edwin H. Armstrong Achievement Award (2016), the Cristoforo Colombo International Prize for Communications (2013), the Copernicus Fellowship (2011) and the *Laurea Honoris Causa* (2008) from the Università degli Studi di Ferrara, and the U.S. Presidential Early Career Award for Scientists and Engineers (2004).